2016

Reactivity of hydroxyl radical: mechanistic insight into the reactivity with dissolved organic matter

Mallika Khare

Michigan Technological University, mkhare@mtu.edu

REACTIVITY OF HYDROXYL RADICAL: MECHANISTIC INSIGHT INTO THE REACTIVITY WITH DISSOLVED ORGANIC MATTER.

By

Mallika Khare

A THESIS

Submitted in partial fulfillment of the requirements for the degree of

MASTER OF SCIENCE

In Environmental Engineering

MICHIGAN TECHNOLOGICAL UNIVERSITY

2016

This thesis has been approved in partial fulfillment of the requirements for the Degree of MASTER OF SCIENCE in Environmental Engineering.

Department of Civil and Environmental Engineering

Thesis Advisor:	*Dr. Daisuke Minakata*
Committee Member:	*Dr. Loredana Valenzano*
Committee Member:	*Dr. David Hand*
Department Chair:	*Dr. David Hand*

Table of Contents

List of Figures

List of tables

Preface

This thesis is submitted as the final work of my research study for Master of Science degree at the Michigan Technological University. It is a documentation on my research that was conducted under the supervision of Associate Professor, Dr. Daisuke Minakata in the Department of Civil and Environmental Engineering, Michigan Technological University, between January 2015 and July 2016.

It presents an insight into the study of reactivity of hydroxyl radical with dissolved organic matter. It was truly a good learning experience as I learnt working with different computational software and handling challenges related to the study.

This work is original to the best of my knowledge. No other thesis nor any substantially similar thesis has been submitted for any other degree or qualification at any other university.

Part of this work that is chapter 2, is prepared in the form of a manuscript and will be submitted to the Environmental Science & Technology journal with minor edits based on the journal policies.

I express my sincere thanks to all who contributed in one way or the other to make this research work a success.

Mallika Khare
15 August 2016

Acknowledgements

I would like to express my sincere and deepest gratitude towards my advisor, Dr. Daisuke Minakata who inspired me to attain perfection in everything I pursue. He was always there to support me in my pursuits and sought only what was the best for me. In these two years of my stay at Michigan Tech, he being an inspiration professionally, also inspired me to lead a disciplined and systematic life. It was an absolute privilege being a part of his research group.

I would also like to acknowledge the support I received from my committee members, Dr. Loredana Valenzano from the Department of Chemistry and Dr. David Hand from the Department of Civil and Environmental Engineering. They were very cooperative and their suggestions helped me in improving my research. I am very thankful for Michigan Tech HPC cluster 'Superior' and Dr. Warren Perger, from the Department of Electrical & Computer Engineering for his support in making this project successful. Also, I would like to thank Dr. Gowtham the Director of Research Computing, Information Technology for helping me with my High-Performance Computing issues.

I would also like to acknowledge the partial financial support provided by the 2015 Ralph Powe Junior Faculty Award from Oak Ridge Associated University (ORAU) for this project.

A person always needs motivation and psychological support to let his best come out in his work. I'm extremely thankful to my parents, Sunil Kumar Khare and Dr. Chetna Shrivastava, my elder brother Peeyush Khare for their immense love and support that kept my confidence alive to complete this work. A very special thanks to my friends Venkata Rajesh Chundru and Mahesh Sanjeev Kulkarni for their immense support.

Abstract

Advanced Oxidation Processes (AOPs) that produce highly reactive hydroxyl radicals (HO•) are attractive and promising water and wastewater treatment technologies because HO• can destroy a variety of organic compounds. However, background dissolved organic matter (DOM) significantly reduces the performance of AOPs by scavenging HO•. The conventional experimental approach to identifying 'average' reactivity limits our mechanistic understanding of the reaction of HO• with complex mixture of surrogate DOM. This is the first study to use quantum mechanical methods to understand the elementary reactions of HO• with a model monomer of DOM. "Temple Northeastern Birmingham model" (TNB). The theoretically calculated aqueous-phase free energies of activation indicate that the functional groups in neighboring positions significantly affect the reactivity of HO• with each active site of the TNB model monomer of DOM.

Chapter1. Introduction

1.1 Significance and Background

The presence of trace level organic chemicals such as pharmaceuticals, personal care products, endocrine disrupting chemicals, pesticides, and herbicides have been found in natural environmental waters. (Snyder S.A. et al., 2003).The concentrations of these chemicals are in the range of nanogram to microgram per liter in water. (Snyder S.A. et al. 2003). The conventional water and wastewater treatment techniques were found to be ineffective in removing these organic chemicals. (Amin M.T. et al., 2014). Improper management and disposal plan of these organic chemicals and their potential adverse effects on human health and natural environment have raised public concern about water.

Dissolved organic matter (DOM) is a heterogeneous surrogate organic that are present in natural environmental waters. The DOM is a combination of both hydrophilic and hydrophobic organic compounds with different functional groups, sizes, and reactivity. (Weng Y.H. et al., 2012). DOM significantly affects the performances of drinking water treatment processes in many ways. For example, by increasing the dose of coagulant required for coagulation process. The coagulant dose is determined based on the turbidity and dissolved organic carbon level which is a measure of DOM. It was anticipated that temperature and climate change affects the formation, properties, and concentrations of DOM. (Ritson et al., 2014). Some of the disinfection by-products produced from the DOM are trihalomethanes such as chloroform, bromodichloromethane, bromoform, and halo acetic acids like mono chloroacetic acid, and dibromo acetic acid.

Advanced Oxidation Process (AOP) is one of the promising and attractive water treatment technologies to destroy trace levels of organic chemicals. AOPs generate hydroxyl radical (HO•), at atmospheric pressure and ambient temperature. The HO• rapidly reacts with the electron rich sites on organic compounds and initiates complex radical chain reactions. There are several factors affecting the performance of AOPs including carbonate species, pH, natural organic matter (NOM), iron, and manganese by scavenging HO• **.** The scavenging of HO• by various factors is measured using quenching ratios (Q_R).

$$Q_R = \frac{k_R C_R}{k_R C_R + k_{NOM} C_{NOM} + k_{CO_3^{2-}} C_{CO_3^{2-}} + k_{HCO_3^-} C_{HCO_3^-} + k_{Fe(II)} C_{Fe(II)} + k_{Mn(II)} C_{Mn(II)}} \quad (1)$$

Following case study was performed on a water source of City of Piqua in Ohio, US that received its water from three surface water sources namely the Piqua Reservoir, Ernst Gravel Pit, and Great Miami River of the City of Piqua. The target organic contaminant to be treated was atrazine and UV/H_2O_2 AOP was used. The quenching ratios due to the effect of carbonate species and NOM were calculated. The quenching ratio obtained by NOM was 0.0056 and by carbonate species was 0.05. The pH of the water was 8.

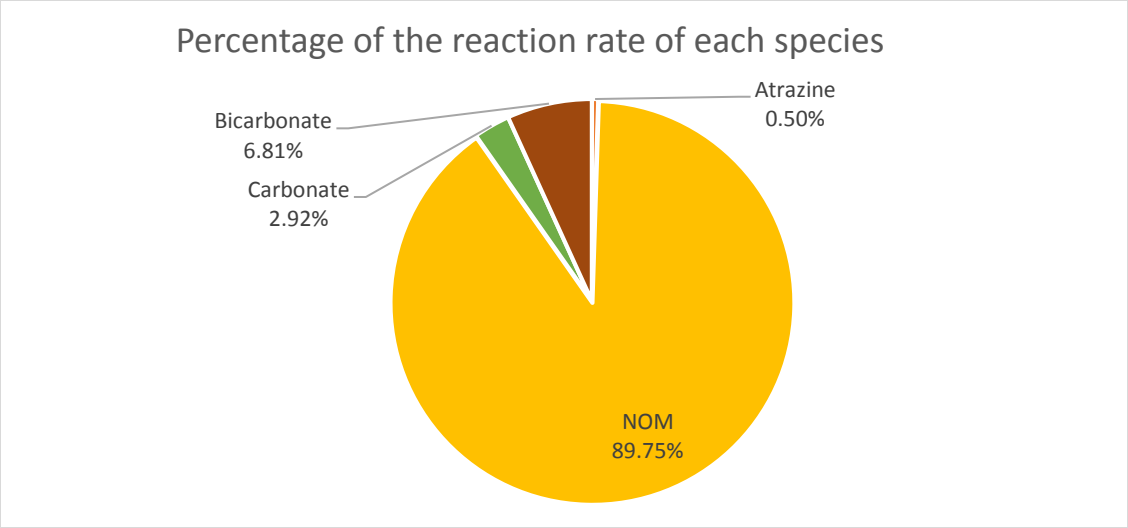

Figure1: Calculated percentage of the reaction rate of natural organic matter, carbonate species and target organic compound atrazine under consideration.
As was seen in Figure 1, the presence of DOM and bicarbonate species are detrimental to the removal of the target organic compound atrazine.

In this thesis, a detailed reactivity of HO• with DOM is studied. Although photochemical and HO• induced reactions with DOM were experimentally studied in the past, detailed mechanisms are not well understood. Until now, experimental studies were focused on obtaining second order reaction rate constants of HO• with various DOM or DOM isolates. ((Westerhoff et al., 2007), (Rosario-Ortiz et al., 2008)).

To perform this detailed analysis, the lowest energy conformer of the TNB model was chosen. The selection of the TNB model for this study was based on the study by Sein et al., 1999 that stated: “TNB is a universal average formula unit of humic acids”. Also, as per the theoretical study on fulvic acid structures by Alvarez-Puebla et al., 2006, “the TNB model of humic acid has some properties similar to fulvic acids like solubility and electronic and vibrational spectra”. TNB model was the simplest structure with a variety

of functional groups attached to it which provided scope for a diverse study for the reactivity with HO•.

1.1.1. Objectives:

The overall goal of this study is to understand the reactivity of HO• with non-specific dissolved organic matter (DOM). It is hypothesized that the quantum mechanical calculations advance our understandings of molecular-level reactivity of HO• with surrogate DOM, which cannot be studied only by the experimental investigations. To test the hypothesis and based on the significance described above, the objectives of this study are:

(i) To establish the methodology of quantum mechanical methods to investigate the initial reactivity of a model monomer of natural organic matter fulvic acid, Temple Northeastern Birmingham model (TNB).

(ii) To calculate the gaseous- and aqueous-phase free energies of activation to compare the HO• reactivity with all the possible reactive sites of the TNB model.

(iii) To calculate the gaseous- and aqueous-phase free energies of interaction to compare the HO• accessibility the possible reactive sites of the TNB model.

1.2. Background Literature Review

1.2.1. Advanced Oxidation Processes

With the advancement in the pharmaceutical technology, water bodies are nowadays accumulating several synthetic organic compounds like pesticides, herbicides, and endocrine disruptors. When not removed, they will have detrimental effects on human

health. To remove these synthetic organic compounds, they are needed to be oxidized into carbon dioxide, water, and mineral acids.

AOPs are found to be the most efficient way of decomposing these organic chemicals. Different types of AOPs used for water treatment includes (1) ozone and UV light, (2) ozone and hydrogen peroxide, (3) UV light and hydrogen peroxide,(4) UV light and TiO2, (5) combinations of all these methods. The HO• utilized in AOPs undergo either hydrogen atom abstraction reaction or rapid addition reaction with the double bonds present in organic compounds. These reaction produces reactive organic radicals that get oxidized rapidly or may utilize dissolved oxygen to form peroxy organic radicals (RCOO.). These organic radicals undergo various chain reactions which lead to the production of a variety of by-products like acetic acid, oxalic acids, formaldehyde, formic acid etc. Out of these carboxylic acids are the most observed by-products because of its low second order rate constants. Several factors that affects the AOPs by reducing the amount of HO• required for the process are (1) carbonate species (HCO3- and CO32-), (2) NOM, (3) reduced metal ions, (4) pH, (5) reactivity of parent component with HO•, and (6) UV light. This study focuses on the reactivity of NOM with HO• in aqueous phase AOPs.

DOM which is the dissolved form of NOM, in UV/H2O2 AOP, interacts with the UV light, scavenges the produced HO• and reduces the efficiency of AOPs. Several studies have been done to analyze the DOM. The photochemical and HO• induced reaction of DOM was also analyzed. Some of these studies are discussed below:

1.2.2 Climatic effects on the formation and properties of DOM

As per the study by Ritson et al., 2014, the areas with heavy rainfall, low sun exposure, organic-rich soils and low evapotranspiration were identified as the prominent sources of DOM in surface waters. These DOM were formed by the decay of plant material or from the agricultural input, urban sources and algal and microbial sources. He explained that the formation of DOM is qualitatively and quantitatively affected by the climate, which leads to variations in the DOM formation. Production of DOM depends on microbial activities which were high in warm temperatures, hence higher DOM production. Moreover, DOM produced in summer were more hydrophilic. Dissolved oxygen in surface waters reduces in summer leads to algal blooms. These algal blooms produced highly proteinaceous DOM which was responsible for more harmful disinfection byproducts (DBPs). Another factor responsible for enhancing DOM production was drought supported by an enzymatic latch mechanism. DOM produced in drought condition were hydrophilic and difficult to be removed by coagulation process. Production of DOM was also affected by erosion and land use management. DOM caused many general and severe problems to the water treatment units. It imparted taste, color, and odor to water. It fouled and blocked membranes and filters, facilitated biological growth in the distribution system, formed DBPs that are harmful to human health. DOM also increases the operational cost of water treatment units by increasing disinfectant demand, coagulant dose, and adjustments required to control pH and decreased filter run time.

Several techniques were used to evaluate the quality and treatability of DOM. SUVA was used to evaluate the aromaticity of DOM, its hydrophobic nature, molecular weight and the formation of DBPs. However, SUVA had limitations as there were some

DBPs precursors in surface waters that could not be observed at 254nm. As per this study, SUVA was found efficient in predicting the formation of disinfection by-products like Trihalomethane (THM) and Halo acetic acids (HAA), whose DBP precursors were obtained from colored humic and fulvic acids. Fractionation was a technique that could be used to access DOM character by charge, hydrophobicity or size. Studies showed that hydrophobic acids were the major contributing factors for the DBP formation. Several processes were designed for the removal of DOM. Coagulation was found to be the most effective technique for DOM removal. Other techniques like pre-ozonation/enhanced coagulation/activated carbon filtration were also effective in DOM removal. Introducing magnetic ion exchange before coagulation was another cost effective technique as it could reduce DBP formation up to 50%. Disinfection processes like chloramination and UV disinfection were found useful as it does not promote THM and HAA formation.

1.2.3 Experimental analysis of reactivity of HO• with DOM

In addition to the study of the DOM character and its removal techniques, it was necessary to understand the reactivity of HO• with DOM in AOPs. Therefore to determine an accurate HO• rate constants with Suwannee River fulvic acid and other DOM isolates, Electron Pulse Radiolysis experiment was conducted by Westerhoff et al., 2007. Seven DOM samples from three sources namely fulvic acid isolated from Suwannee River, purchased from International Humic Substances Society, three forms of DOM isolates from lake Saguaro, AZ (hydrophobic acid, hydrophobic neutral and transphilic acid) and three forms of DOM isolates from waste water treatment plant (hydrophilic neutral, transphilic neutral and transphilic acid) were taken. A solution was prepared using

dehydrated DOM and buffered (10mM phosphate) nanopure water. This solution was treated with radiations of linear accelerator electron pulse radiolysis system from the Department of Energy Radiation laboratory, University of Notre Dame. This lead to the production of HO•, hydrated electrons and hydrogen atoms. Using the transient absorption results obtained from $1.0x10^{-2}$ M KSCN solution at 475nm, the doses of 3-5 Gy/4-5 ns pulse were used. The biomolecular reaction rate constants were determined using two different techniques. With the first technique it was observed that with the increase in the concentration of DOM, the absorbance of $(SCN)^{2-}$.decreased and the rate constant yielded was $k_{HO\bullet\text{-}DOM} = (1.55\pm0.04)x10^{8}\ M^{-1}s^{-1}$. With the second technique i.e. by direct measurement technique, it was observed that $k_{HO\bullet\text{-}DOM}$ at 272nm was found to be $(1.87\pm0.07)\ x10^{8}\ M^{-1}s^{-1}$ and at 400nm was found to be $(1.39\pm0.16)\ x10^{8}\ M^{-1}s^{-1}$. The average $k_{HO\bullet\text{-}DOM}$ value with Suwannee River fulvic acid obtained was $(1.6\pm0.24)\ x10^{8}\ M^{-1}s^{-1}$.For other DOM isolates the $k_{HO\bullet\text{-}DOM}$ values ranged from $(1.45\pm0.02)\ x10^{8}\ M^{-1}s^{-1}$ to $(4.53\pm0.54)\ x10^{8}\ M^{-1}s^{-1}$.

Rosario-Ortiz et al., 2008 studied the HO• rate constant with Non-isolated Effluent Organic Matter (EfOM). EfOMs were also found to reduce the overall efficiency of the AOPs. These EfOM were a combination of NOM, soluble microbial products (SMP) and harmful chemicals. Since the previous studies on HO• reaction rate constants were focused on the isolated NOM, hence it was stated that isolation of NOM might change its original properties and it might influence the values of the rate constants. So, it was important to estimate an accurate value of $k_{HO\bullet\text{-}EfOM}$ with non-isolated samples and also to check if these values vary with the treatment and locations. In the duration of two months july and august 2007, eight water samples were collected from different locations namely Florida,

California, Nevada, Colorado, and Arizona. Electron Pulse Radiolysis method was used to get an accurate HO• reaction rate constant. The rate constant values varied from (0.27±0.01) $x10^9$ $M^{-1}s^{-1}$ to (1.21±0.17) $x10^9$ $M^{-1}s^{-1}$ for 8 different samples. The average value of $k_{HO\text{-}EfOM}$ calculated was (0.87±0.36) $x10^9$ $M^{-1}s^{-1}$. These values were compared with the different NOM isolates values and it was concluded that EfOM is more complex structures than their isolates.

Concentrations of DOM and its reactivity within certain time varies with the environmental conditions. Rosario-Ortiz et al., 2007, studied the characterization of DOM under varying ambient conditions. Four main tributaries of Lake Mead were considered for this study namely Las Vegas Wash (LVW), Muddy River (MR), Virgin River (VR) and Upper Colorado River (UCR) and an extra sample from Lower Colorado River (LCR). This study was also performed to analyze the variation in DOM characteristics within each water source. The DOM samples from each source were evaluated on the basis of size, polarity and fluorescence analysis. Specific Ultraviolet Absorbance (SUVA) values were used to differentiate DOM of different origins. On comparison, it was found that higher SUVA values associated with the lakes and streams were influenced by the agricultural inputs, runoffs, and snowmelt. Lower aromatic nature of DOM was reflected by the lower SUVA values. In tributary LCR, DOM was observed to be constant for a year with an average SUVA value of 1.0-1.5 $Lmg^{-1}m^{-1}$. This indicated lower aromaticity of DOM in LCR with increased hydrophilicity. Consistency in SUVA value indicated that detention time in Lake Mead allows mixing and brings down reactions to equilibrium. The site UCR had SUVA values ranging from 1 to 4.5 $Lmg^{-1}m^{-1}$. Samples were collected during the period of June 22, 2005, to October 19, 2005, and SEC chromatograms were obtained for

samples collected on October 19, 2005. Fractions were defined from 1 to 5 based on the highest molecular weight at 1 and fraction 5 at the lowest molecular weight. Fraction 1 peaks were observed for sites VR, MR, LVW confirming the presence of high molecular weight DOM at these sites. This fraction was not observed for sites UCR and LCR showing a lack of higher molecular weight of DOM. Fraction 2 was observed in all samples. Fraction3 was observed for samples at VR, LVW, and MR. Fraction 4 was observed in sites VR and LVW at its highest intensity. However, this analysis had the limitation that it detected DOM within the range of UVA 254nm and failed to quantify non-chromophoric DOM. Samples collected on June 22, 2005, were further studied. Site MR revealed the widest molecular weight distribution while site LCR showed the narrowest molecular weight distribution. Fluorescence analysis was conducted on all samples and EEM spectra was observed with one peak at the 310-340nm excitation wavelength. Site LVW showed the largest contribution from aromatic proteins and microbial by-product.

Reactivity of HO• with organic matter also depends on temperature. This reactivity with the variation in temperature was experimentally analyzed by McKay et al., 2011. The reaction that occurred between HO• and organic contaminants were mainly by hydrogen atom abstraction or addition to an aromatic ring. These reactions were very fast with k HO• $\sim 10^8 - 10^{10}$ $M^{-1}s^{-1}$. Earlier, the studies mainly focused on the reactivity of organic matter with HO• But, this study also focused on the reactivity of effluent organic matter. The reaction rate constants $k_{NOM\text{-}HO\bullet}$ and $k_{EfOM\text{-}HO\bullet}$ gives the overall reaction rate constant value of the reaction. Many studies have been done on the reaction between HO• and organic

matter but this study focused on the dependence of these reactions between HO• with both NOM and EfOM on temperature. For this study, three NOM isolates namely Elliot Soil humic acid (ESHA), Pony Lake Fulvic acid (PLFA), Suwannee River standard fulvic acid I (SRFA) and three EfOM samples were utilized. The apparent activation energies (Ea) and transition-state entropy (ΔS) were calculated using temperature dependent kinetic data. For the calculation of the reaction rate constant, the linear accelerator electron pulse radiolysis facility in the University of Notre Dame Radiation Laboratory was used. N_2O gas was used to pre-saturate the NOM and EfOM solutions, so as to isolate HO• on radiolysis. It was observed that the $k_{NOM\text{-}HO\bullet}$ values for NOM isolates varied from (1.21-6.90) x 10^8 $Mc^{-1}s^{-1}$. From these results, it was concluded that the NOM reactivity with hydroxyl radical depends on upon the source of formation of NOM. Arrhenius plots were made for ESHA, SRFA and PLFA and linear plots were observed, which clearly represented the independence of structural changes of NOM isolates with the change in temperature (temperature range under study). The values of apparent activation energy for PLFA, SRFA and ESHA obtained were 15.18, 14.42 and 29.93 kJ mol^{-1} respectively with a very minute difference of 2 between SRFA and PLFA. Since, ESHA had the greatest aromatic carbon content and was also a humic acid as compared to the other two which were fulvic acids, the disaggregation of ESHA would lead to the greater apparent activation energy. The average rate constant values for EfOM were greater than that of NOM values. The values obtained at room temperature ranged from (6.79-9.37) x 10^8 $Mc^{-1}s^{-1}$. In general, the standard deviation values were observed to be larger for EfOM than NOM considering the fact that EfOM could disaggregate at higher temperatures due to the heterogeneity of the EfOM.

It was important to study the effect of EfOM in the HO• radical scavenging as the difference in the composition of EfOM would impact the AOP significantly. EfOM was a composition of background NOM, soluble microbial products (SMP) and natural and synthetic trace chemicals.

Dong M. et al., 2010, studied the reactivity of effluent organic matter (EfOM) with hydroxyl radical as a function of molecular weight. The reactivity of EfOM with HO• was evaluated at different wastewater treatment sites using an empirical equation. The equation showed that $k_{EfOM\text{-}HO}$ is a function of specific UV absorbance at 254nm, fluorescence index, the weight average molecular weight (Mw) and dispersity d. On further analysis, it was found that differences in Mw of EfOM played an important role in predicting the value of $k_{EfOM\text{-}HO}$. This study focused on determining $k_{EfOM\text{-}HO}$ as a function of apparent molecular weight (AMW) for different wastewater effluents to understand the source of variability. Four samples were used from three sites A, B and C of the wastewater treatment facilities in the United States. Site A involved aerobic and anoxic conditions with nitrification/denitrification, site B utilized anaerobic conditions with nitrification/denitrification. Site C had two different treatment trains. So, two samples were collected. Site C1 used nitrification/denitrification, however, site C2 does not use nitrification. Samples were sent to Radiation Laboratory of the University of Notre Dame and were analyzed within one month. To calculate $k_{EfOM\text{-}HO}$, linear accelerator (LINAC) electron pulse radiolysis facility at the Radiation Laboratory, University of Notre Dame was used. For individual water samples, $k_{EfOM\text{-}HO}$ values were evaluated with similar runs.

Average Dose of 3-5 Gy per 3-4 ns pulse was used with 1x 10^{-2} M KSCN solution at λ= 475nm. EfOM fractions were obtained for bulk, <10kDa, <5kDa, <3kDa, and <1kDa for all the sites. The bulk samples rate constants obtained were ranging from 6.32 to 14.1 x10^{8} $MC^{-1}s^{-1}$. The <1kDa fractions had relatively higher rate constants ranging from 14.3 to 35 x 10^{8} $MC^{-1}s^{-1}$. The kEfOM-OH values for fraction <3kDa were ranging from 10.6 to 23 x 10^{8} $MC^{-1}s^{-1}$ and for <5kDa it ranged from 7.6 to 16.2 x10^{8} $MC^{-1}s^{-1}$. For <10kDa the values ranged from 6.7 to 18.5 x 10^{8} $MC^{-1}s^{-1}$. With the obtained scavenging rates it was found that out of all the fractions,60% of the scavenging was due to the <1kDa EfOM for all the four sites. The increased reactivity observed from the k_{EfOM} values shows the production of the soluble microbial product (SMP) when reacted with HO• that varies with the wastewater treatment process.

Decomposition of several organic contaminants takes place in the presence of reactive organic species like HO•, singlet oxygen (O_2), superoxide ($O_2.^-$), hydrogen peroxide (H_2O_2) etc. The production of HO• and O_2 from photochemical reactions in natural waters was observed after the confirmation of production of H_2O_2 photochemically in marine waters in 1966. Temperature dependence of the photochemical formation of HO• from dissolved organic matter (DOM) was studied by McKay et al., 2015. When DOM undergoes photolysis, HO•, O_2, H_2O_2, DOM*(triplet state) and $O_2.^-$ were produced. The DOM in ground state absorb a photon and undergoes internal conversions and forms DOM* whereas H_2O_2 is formed by the disproportionation of $O_2.$-. HO• is a result of multiple reaction pathways. The steady state concentration of HO• was found to be around 10^{-18} to 10^{-16} M in natural waters being highly reactive. Apparent quantum yield reported for HO• was in the range of 10^{-4} to 10^{-5}, higher for waste water. The reaction mechanisms

behind the formation of HO• from the photochemical source DOM was explored in this study. The two possible pathways for the generation of HO• were described as under:

(i) H_2O_2 dependent -it includes photo-Fenton reaction and direct photolysis of photochemically produced H_2O_2. This pathway decreases the HO• production by 50% for some samples when catalase is used to decompose the H_2O_2 produced photochemically.

(ii) H_2O_2 independent – in this pathway, the species present produces free HO• and low energy hydroxylating species. For the production of free HO•, H-atom abstraction from water by DOM at its excited state is observed to be one of the mechanisms but yet not confirmed.

In this study, the temperature dependence of quantum yield, Φa for bulk DOM isolates was investigated with and without the presence of catalase and apparent molecular weight fractions.

For reference and comparison of the results obtained, the temperature dependence of the photolysis of p-benzoquinone was also studied. DOM isolates chosen for testing were: Suwannee River fulvic acid I (SRFA1S101F), Suwannee River humic acid II (SRHA 2S101H), Suwannee River NOM (SRNOM, 2R101N) Pony Lake fulvic acid (PLFA, 1R109F), and Elliot Soil humic acid (ESHA, 1S102H), all purchased from International Humic Substances Society. Irradiation experiment was carried out to achieve measurable HO• concentration for 2.5-8h using an Oriel 1429A Solar Simulator equipped with a 1000W xenon lamp.

Temperature dependence of Phenol yield from Benzene

An HO• probe benzene was used by the formation of phenol when cyclohexadienyl radical reacts with dissolved oxygen under the Dorfman reaction. To fetch HO• radicals, 3mM of benzene concentration was used. Average yield Y_{Phenol} obtained from the experiments that were conducted in the temperature range of 11.6 to 38.4°C was 0.63±0.07 without any apparent temperature dependence. An activation energy value of 16.6±5 kJ mol^{-1} was observed during the production of HO• from nitrate photolysis. This value was compared with the value 19±4 kJ mol^{-1} of experiments conducted by Chu and Anastasio in 2003 and 16±4 kJ mol^{-1} obtained by Zellner et al. in 1990. The Y_{Phenol} values ranged from 0.43-0.95 at different pH. (Sun et al., 2014) determined this value as 0.69. The limitation related with this study was that the quantum yield for HO• obtained from the irradiations performed using solar simulator was intensively wavelength dependent. So, the quantum yield obtained should be read as an average quantum yield of the spectral output of solar simulator at λ >290nm.

Temperature Dependence for Bulk DOM isolates

It was observed that the apparent activation energies obtained for DOM isolates ranged from 16 to 34 kJ mol^{-1}.There was a little variation in the value of activation energy of the DOM isolate SRFA and is equal to (34.3±7.2kJ mol^{-1}). This reflected that there was consistent production of HO• .The activation energies in the range of 16 to 18kJ mol^{-1} for DOM isolates ESHA, SRHA, and SRNOM shows diffusion-controlled reactions.

Temperature Dependence of p-Benzoquinone Photolysis

In this, an experiment was conducted, in which 92.5μM of p-benzoquinone was utilized to produce 500nM phenol in an irradiation exposure for 12 mins. From the reaction, it was observed that phenol that formed from the irradiation of p-benzoquinone had benzene that might be influenced by the hydroxylation by other species apart from free HO•. Since, it is believed that DOM contains compounds like quinones, the presence of low energy hydroxylation in irradiated DOM can be considered. It was concluded that an increase in temperature supports in the production of hydroxy-p-benzoquinone and hydroquinone up to temperature 23°C whereas on further increase in temperature leads to dissociation of the complex. From the experiment, it was concluded that the activation energies observed for HO• production from DOM is not completely based on photolysis of quinone.

The overall removal efficiency of HO• in AOPs was variable and it depends on many factors like its location in the treatment train, the water quality, and type of contaminants present. Many dissolved organic contaminants did not react with 100% efficiency. Moreover, this complexity increased if there were other dissolved substances present additionally.

To understand the contaminant destruction in AOPs, it was important to evaluate both HO• reaction efficiencies and reaction rate constants. The combination of the HO• reaction efficiency with reaction rate constant formed an effective contaminant removal parameter (ECRP) for a contaminant. Effective contaminant removal rate constant (ECRC) was defined as a measure of speed and permanent transformation of the HO• reaction.

Reaction efficiencies less than 100% may undergo "repair" reactions, where some of the intermediate species will regenerate the parent contaminants. Many HO• reaction efficiencies were found for the single component aqueous system, but efficiencies of mixtures of contaminants were yet to be investigated. Satinder A. et al., 2013 studied the HO• rate constant and determined the efficiencies of a single component and multicomponent mixtures. Experiments were conducted in pure water to get reaction efficiencies, and in treated waste water to get overall removal efficiencies. Steady State radiolysis experiment was performed to produce HO• in water. It was carried out by decomposing water molecules in different aqueous solutions with chemical contaminants of single or mixtures of compounds. The solution irradiations were carried out using a 60Co Gamma cell 220 gamma irradiation, stationed at the Radiation Laboratory, University of Notre Dame. The average dose rate of 0.0029 $kGymin^{-1}$ was used during irradiation.

Deionized water greater than 18MΩ-cm were used to prepare solutions. Also other methods like filtered secondary wastewater or reverse osmosis permeate obtained from Advanced Water Purification Facility (AWPF) of Orange County Water District in Fountain Valley, CA were used to prepare solutions.

In N_2O-saturated solution experimental yield of HO• was found to be 0.59 $umolJ^{-1}$. Pulse Radiolysis experiment was used with short pulses of (2-3ns) of 8Mev energy electrons from a linear accelerator (LINAC) to produce HO• radicals. LINAC was available at the Radiation Research Laboratory of the University of Notre Dame. The dose absorbed by the solution could be evaluated using standard N_2O saturated $1x10^{-2}$ M KSCN

solutions at λ=475nm (GE= $5.2x10^{-4}m^2J^{-1}$) with average doses of 3-5 Gy per 2-3ns pulse corresponding to 2-3uM HO• radicals produced per pulse. Change in concentration of contaminant compound was analyzed in solution from Water HPLC system using gamma irradiations known as HPLC analysis. Removal Efficiencies of HO• for the organic compounds was analyzed by plotting a graph between absolute change in contaminant concentration (mM) with absorbed radiation dose in kGy units. Contaminant loss of ≤ 30% was accounted to prevent interference of intermediates produced during the reaction by fetching HO•. Removal efficiency was calculated by dividing initial slope by 0.59 mmol J^{-1}. The value 0.59 mmol J^{-1} determined the total HO• yielded under N_2O saturated conditions. In pure water with only one solute, this would be the reaction efficiency.

The HO• rate constant and HO• reaction efficiency were the two important experimental parameters used to determine effective contaminant removal parameter for four compounds sulfamethoxazole (SX), biphenol-A, caffeine and N, N, diethyl-3-methyl benzamide. The HO• rate constants experimental values obtained were (6.9±0.4) $x10^9$ $M^{-1}s^{-1}$ for caffeine and (8.5±0.3) $x10^9$ $M^{-1}s^{-1}$ for sulfamethoxazole and (4.9±0.2) $x10^9$ $M^{-1}s^{-1}$ for DEET and (6.9±0.3) $x10^9$ $M^{-1}s^{-1}$ for BPA. The variation in reaction efficiency values in pure water of these compounds showed that there were differences in mechanistic pathways. The HO• was mainly scavenged by carbonate and bicarbonate ions in wastewater, dissolved organic matter and metal ions. So, understanding removal efficiencies in the presence of dissolved organic contaminants was important. For mixtures of contaminant, efficiencies were evaluated experimentally in deionized water and in highly treated, osmosis filtration treated wastewater. HO• generated from irradiations were used to treat a mixture of 25uM of each DEET, caffeine and sulfamethoxazole and each

removal constants were calculated. Removal efficiencies of 27%, 29%, and 29% were observed for DEET, caffeine and sulfamethoxazole. A mixture with 50uM of same three dissolved organic compounds in deionized water when subjected to HO•, similar efficiency values were obtained. When highly RO treated wastewater was used to perform the same experiment, the value of sulfamethoxazole lowered slightly, however DEET and caffeine values were consistent with deionized water mixtures. Effective contaminant removal rate constants were evaluated to elaborate the leveling effect of HO• removal efficiencies calculated from mixtures data. HO• reacted 20% faster with sulfamethoxazole because its rate constant was slightly greater than caffeine and DEET. However, it does not completely react and form stable measurable compounds. Half of the radical HO• adduct forms an unstable product. Hence, sulfamethoxazole scavenges more HO• radical as compared to caffeine or DEET. On carrying out experimental studies by varying the concentration of mixtures and modeling, it was concluded that reactivity of transient species and finally oxidized products were important to better analyze the overall chemistry.

1.2.4 Structure of natural organic matter

Further, in addition to experimental analysis, the structures of NOM were explored. NOM structures were not clearly defined due to their molecular structural complexity. Attempts were made to determine components of NOM through chromatographic and mass spectrometric resolution but were not a success. Leenheer 2007, in his paper, summarized an overview of the model structures approximated till the time that would help to develop molecular structures of NOM. The basis of NOM models was humification which

produced humus, fulvic acid, humic acid, humin and subfractions like glucic acid, ulmic acid etc. Here humic subfractions were believed to be pure compounds. Fuchs and Flaig developed humic acid models that were highly aromatic phenol structures. Based on the studies it was stated that the humic substances were formed by the reaction between reducing sugars and amino groups of proteins under abiotic conditions to produce melanins. It was concluded that humus has a heterogeneous macromolecular structure as per the obtained humus precursor structures like lignin from extensive condensation reactions. It was impossible to determine the possible structure of NOM. Further, analytical models were developed using degradative techniques and nuclear magnetic resonance (NMR). With the degradative techniques using gas chromatography and spectrometry lignin-derived phenols, aliphatic acids, amino acids, amino sugars and neutral carbohydrates were obtained in soil and water as significant components of NOM. The NOM structures obtained by NMR spectra had a higher percentage of aliphatic nature and a lower percentage of phenol content. Electrospray ionization/mass spectroscopy (ESI) was another analytical technique used to qualitatively study the model structures of NOM. In this method, the ion cyclotron resonance mass spectrometer was used with an ultra-high resolution to find molecular formulas of 4626 molecules of Suwannee river fulvic acid. Further, six successive models of Suwannee river fulvic acid were approximated. The first model confirmed that fulvic acid is rich in both aliphatic and aromatic structures with an average of four carboxylic acid groups per molecule. However, nitrogen, sulfur and phosphorus were not included in the study considering them as minor elements. The second model was a result of quantitative estimation from a two –stage normal phase chromatography of SRFA on silica gel. With this model pKa value of 2 and lower were

recorded confirming strong acid character due to the presence of carboxylic acid. The third model was comparatively higher in molecular weight, phenol content, and carboxylic acid groups. The fourth model was obtained by separation of negative ions of SRFA from electrospray ionization/multistate mass spectrometry. This model revealed that it had a lignin precursor because of the formation of o-dihydroxy benzene as the final product ion. The fifth model recorded a very high pKa value of 0.5 with an average composition of 5 carboxylic groups per molecule. This model led to the consideration of diagenetic reaction sequence due to the presence of electrostatic field effects generated by the carboxylic acid groups. The sixth model was studied by normal phase and reverse phase fractionation on XAD-8 resin. Tannin and terpenoid with lignin in small amount were found to be the precursors of the SRFA as per the C-NMR, infrared and ESI/MS characterization. In addition to these models, dissolved organic matter diagenesis models were also studied. A fulvic acid was fractionated on XAD-8 resin from tannins. This model had its exterior surrounded by carboxylic acids and hydroxyl groups that made it water soluble and a hydrophobic interior that reacts with the XAD 8 resins.

1.2.5 Minimum energy conformer of natural organic matter

After obtaining different models of humic and fulvic acids, conformational modeling of these models was also studied to determine the lowest energy conformers of the models. Sein T. L et al., 1999 studied the two humic acid-base structures, the Steelink structure, and Temple Northeastern Birmingham model. This study involved the analysis of structural diversity in terms of conformational isomerism of the building block structures

of humic acid namely Steelink Model and Temple Northeastern Birmingham Model (TNB).

As per the standard method, generally, the molecular modeling was done following a cycle of minimizing the energy of a trial geometry, then studying the molecular dynamics of that particular molecule to find if any conformers exist and then minimizing the conformers to identify the lowest of all. For complex structures, this method was found to be inefficient in terms of altering torsional angles of the geometry, interatomic distances, and coordinates of the atoms of the molecules. Different methods have been developed to overcome the problems stated above. Deterministic methods and, stochastic methods (pseudo)randomly varied in interatomic distances, coordinates, and torsional angles to generate molecular geometries. Inversion of chiral centers was an important condition to be understood about an unknown stereo chemical configuration and was covered by random searching methods. A conformational problem different from the ones stated above arose when the absolute and relative chiral configuration of the humic acid monomer was not known, unlike proteins, polypeptides and polysaccharides. So, a search for a proper conformational method allowing chiral inversion became essential. For biological materials like humic acids, low energy conformers were obtained using multiple searching methods and molecular dynamics. The basic humic acid building block structures were produced with the help of the Sketch utility of Sybyl (Tripos). Tripos force field and the Fletcher-Powell conjugate-gradient minimization algorithm were used to optimize the 64 different stereoisomers of Steelink model of humic acid. Random conformational search was started using Sybyl for the five lowest energy stereoisomers. New conformers were obtained by making variations to coordinates of the geometries, retaining structures with

reasonable energy, optimizing the structure, and repetition to obtain a "duplicate" structure. From this process, the lowest energy structure was further investigated by molecular dynamics. For this, RIPS algorithm of Houk et al. was used as reported by Lawrence T. Sein et al 1999. This procedure was adopted for TNB model as well. The initial geometries for TNB structure analysis were obtained from the minimized Steelink structures. Molecular dynamics study involved a constant temperature of 300 and 400K for 20 ps with TRIPOS and MM+ force fields. For Solvation model, the study was conducted using a box of 1738 water molecules periodically.

Finally, the molecules were slowly heated to 600K from 300K and then reducing the temperature back to 300K over 10ps. Quantum Mechanical calculations were performed using the HyperChem suite of programs. PM3, semi-empirical techniques were used to perform calculations on both the Steelink model and TNB model of humic acid and single point energies were calculated. Out of all the configurations, the RSSRSSR=SRRSRRS was recorded consistent with the lowest energy. For checking the stability of the result, it was tested by varying two critical torsion angles for TNB model. The TNB structure was thus stated to be the universal average formula unit of humic acid. This modeling study investigates the relative energies of all the stereoisomers of humic acid building block structure. This conformational structure was found to be 2-4 kcal/mol more stable than the other lowest energy species. Two important features to be noted of all RSSRSSR configurations were as follows:

(i) Aromatic ring provides van-der-Waal stability.

(ii) Two carboxylate groups attached on the same side adjacent to each other showing the possibility of metal binding.

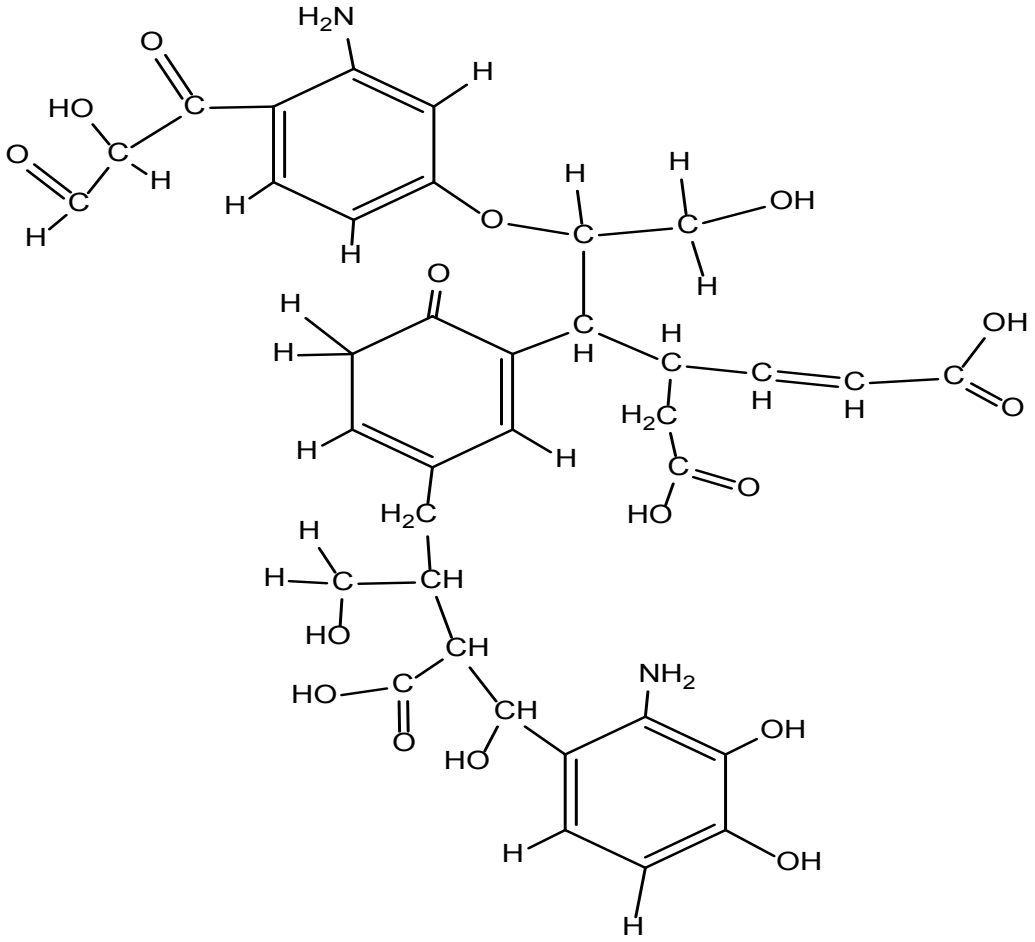

Figure 2: Molecular structure of low-energy TNB HA conformers as determined by RIPS search.

For TNB minimization, 10 lowest energy stereoisomers of Steelink64 were used, being structurally similar. These structures were observed under molecular dynamics protocols which showed no significant difference in terms of relative energies and conformational features.

The conformational stability was investigated using the semi-empirical quantum mechanical method. Since only a single low energy stable stereoisomer was obtained from

molecular modeling of humic acid, this quantum mechanical method was used to develop potential energy surface for torsional movements. And based on this study, we included TNB structure of humic acid for our study.

1.2.6 Theoretical studies on reactivity of HO• with organic compounds in aqueous phase

In addition to experimental studies, many theoretical studies have been performed to analyze the reactivity and interaction of different organic compounds with hydroxyl radical in the aqueous phase. Minakata D. et al., 2014 developed a linear free energy relationship (LFER) for reactions between radicals in the aqueous phase. A total of 101 compounds were involved in setting up this relationship. Out of these, 15 were aromatic compounds that underwent the HO• addition reaction, 67 were carbon-centered radical compounds that went through O_2 addition, 10 were peroxyl radicals undergoing disproportionation and 9 were peroxyl radicals with unimolecular decay. Aqueous phase reaction rate constant of HO• addition to aromatic compounds was evaluated by first calculating the reaction rate constants from aliphatic chains associated with the compound using the group contribution method and further by subtracting this rate constant from the experimentally obtained reaction rate constants for that specific compound. The compounds used for establishing LFER had a single functional group in it. The LFER relationship obtained for aromatic compounds was ln kchem = $-0.14\ \Delta G^{act}_{aq,calc} + 20.60$ with 15 rate constants. The standard deviation of 0.5 was obtained which implied that 0.19% of the cumulative probability of the data was distributed and varied (plus or minus) more than

one standard deviation from experimental result when considered normally distributed. Further, the LFER relationship for the addition of O2 to carbon-centered radicals in aliphatic chains obtained was ln k_{chem} = -0.088$\Delta G^{act}_{aq,calc}$+ 19.93 with 19 rate constants. The standard deviation of 0.31 was obtained as per calibration and 1.05 for prediction. This implied that 0% of the calibration data and 67% of the predicted data varied plus or minus more than one standard deviation from experimental values. Similarly, the LFER for the disproportionation of peroxyl radicals was obtained as ln k_{chem} = -1.14$\Delta G^{act}_{aq,calc}$ +27.09 with 10 reaction rate constants. The standard deviation for this relationship was 0.62 which means 14.7% of the data varied plus or minus more than the standard deviation obtained from experimental values. For the unimolecular decay of peroxyl radicals, the LFER reported was ln k_{chem}¬ = -0.39$\Delta G^{act}_{aq,calc}$+ 13.00 when 9 reaction rate constants were used. The standard deviation of 3.2 implying that 99.7% of the values varied by plus or minus more than the standard deviation of experimental values. This methodology was claimed to be useful to predict the formation of the intermediate radical species and the byproducts in the aqueous phase advanced oxidation systems.

In addition to this, Minakata D. et al., 2015 carried out an experimental and theoretical study on the reactivity of hydroxyl radical with multiple carboxylated and hydroxylated benzene compounds in the aqueous phase. Using Electron Pulse radiolysis experiment at Notre Dame Radiation Laboratory and theoretical analysis using ab initio quantum mechanical calculations with Gaussian09 revision D.02 at Michigan Tech high-performance cluster “Superior”, Minakata D. et al., produced the results. This study

focused on the investigation of aqueous phase HO• reaction with multiple carboxylated and hydroxylated benzene compounds by comparing the experimental and theoretical results of kinetic rate constants, thermochemical properties, and transient spectra.

For HO• addition to various multiple carboxylated benzene compounds, experimental reaction rate constants and theoretical values of $\Delta G_{aq,calc}^{act}$ were obtained from the addition of HO• to carboxylated and hydroxylated benzene compounds. A decrease in the reaction rate constant value was observed on increasing temperature when $\Delta G_{aq,calc}^{act}$ were found negative. In such cases forward reactions were found possible but, the entropy of the reactants and the reaction was not suitable. In addition to this, negative values of $\Delta G_{aq,calc}^{act}$ were obtained on the reaction of HO• with aromatic compounds in aqueous phase using single functional groups.

The Linear Free Energy Relationship (LFER) obtained for HO• reaction with multiple carboxylated and hydroxylated benzene compounds in this study was as follows:

$$\ln k_{chem} = -0.14\Delta G_{aq,calc}^{act} + 20.30 \ (n=15) \qquad (2)$$

where k_{chem} is the chemical reaction rate constant, obtained from overall experimental rate constant. A total of 14 multiple hydroxylated and carboxylated benzene compounds were considered under study. The time dependent- density functional theory study was carried out to analyze the transformation hydroxy cyclohexadienyl radicals undergoes initially with HO• in the aqueous phase and also to examine the stability of HO-adduct formed. At first, aqueous phase optimized transition state structures were obtained using DFT. Then, the effect of the functional groups that created transient spectral peaks at nearly 250 and 350 nm was studied by analyzing the molecular orbitals of the optimized

transition state structures. For the several reactive sites of the benzene ring that HO• can attack, the overall $\Delta G_{aq,calc}^{act}$ was calculated using Benson's thermochemical additivity principle given by:

$$\Delta G_{aq,calc}^{act} = \Sigma \Delta G_{aq,calc}^{act(i)} \quad (3)$$

where i is the position on the benzene ring where HO• can attack. For HO• reaction with benzoate and benzoic acid, different transient spectra were obtained at reaction times of 1, 5, 50 and 100 μsec at pH of 6.9. Those spectra reflected that at a wavelength of 330 nm, peak absorbance is observed and decreases as the reaction proceeds. When the absorbance decreases significantly after 100μs of reaction between 320 nm and 340 nm, generation of an intermediate radical called hydro cyclohexadienyl is confirmed.

According to the theoretical study using TD-DFT method, it was observed that peaks obtained at wavelength 322 nm and 324 nm were due to the addition of HO• to the ortho and para positions of benzoate and the peak of the transient spectra was also found at 330 nm. However, when the HO• was added to the meta position of the benzoate, two peaks were observed at wavelength 326 nm and 246 nm.

The study was further moved to multiple carboxylated benzene compounds like phthalic acid(1,2-dicarboxylic acid), terephthalic acid (1,4-dicarboxylic acid), trimesic acid(1,3,5-tricarboxylic acid), pyromellitic acid (1,2,4,5- tetracarboxylic acid), and 1,2,3,4,5-pentacarboxylic acid. The decrease in the experimental rate constants was observed with the increase in the number of carboxylate functional groups. The theoretical free energy of activation calculated gives information about the effect of a number of

carboxylate functional groups and their positions (benzene ring) on the reactivity of HO•. The observed change in free energy of activation for different acids are as follows:

ΔGaq,calcact : phthalic acid at position 3 = -4.85 kcal mol^{-1}

Phthalic acid at position 4= -3.00 kcal mol^{-1}

Terephthalic acid at any position = -7.61 kcal mol^{-1}

Based on these result, the change in free energy of activation of terephthalic acid was smaller than phthalic acid. When there were three carboxylate groups attached at position 1, 3, and 5 of the benzene ring, the $\Delta_{Gaq,calc}{}^{act}$ observed was equal to -6.12 kcal mol^{-1} for HO• to attack at position 2,4,6. The reaction rate constant of HO• reactivity with terephthalic acid was found to be $(4.0 \pm 0.1) \times 10^9$ $M^{-1}s^{-1}$ which is nearly similar to the experimentally recorded value of $(4.95 \pm 0.28) \times 10^9$ M^{-1} s^{-1}.

The reactivity of HO• was studied with mono-hydroxylated benzoic acids such as salicylic acid(2-hydroxybenzoic acid), 3-hydroxybenzoic acid and 4-hydroxybenzoic acid), dihydroxybenzoic acids(2,3-,2,4-,2,5- and 2,6- dihydroxybenzoic acids) and tri-hydroxybenzoic acids (2,3,4- and 3,4,5-tri-hydroxybenzoic acids). The overall reaction rate constants obtained experimentally for the hydroxylated benzoic acids are greater in value than those for the multiple carboxylated benzene compounds. This is due to the fact that hydroxyl functional groups support the reactivity of HO• to a significant extent. Based on the experimental observation dihydroxybenzoic acids reaction rate constant is larger than tri-hydroxybenzoic acids. The change in free energy of activation (ΔGaq,calcact) for all hydroxybenzoic acids was in the range of -13.0 kcal mol^{-1} to -18 kcal mol^{-1}. But, for salicylic acid it was -23.4kcal mol^{-1}.

1.2.7 Universal Solvation Model-SMD

A continuum solvation model which involved quantum mechanical charge density of solute interacting with a continuum solvent was presented by Marenich V.A. et al, 2009. The continuum solvent was defined by a bulk dielectric medium and atomic surface tensions at the boundary of solute and solvent. The Solvation Free Energy was divided into two main components: (i) bulk electrostatic contribution arising from self-consistent reaction field (SCRF) treatment. In this nonhomogeneous Poisson equation solution was utilized for electrostatics in the form of integral equation formalism polarizable continuum model (IEF-PCM), (ii) Cavity dispersion solvent structure term.

The free energy of solvation at standard state was divided into the following components:

$$\Delta G^{\circ}s = \Delta G_{ENP} + G_{CDS} + \Delta G^{\circ}conc \quad (4)$$

Where ENP stands for electronic (E), nuclear (N) and polarization (P) components of free energy. The nuclear component of ENP equals to:

Total Energy (g) calculated at gas phase equilibrium structure – Total Energy (g)¬ calculated at liquid phase equilibrium structure.

If the geometry of the molecule was considered same in gas and liquid phase, then ENP gets reduced to EP since all calculations carried out were associated with gas phase and the nuclear term was assumed zero here. In ΔG_{CDS}, CDS stands for the solvent cavitation (C), changes in dispersion (D) energy and possible changes in solvent structure (S) and ΔGconc corresponds to the concentration change in gas and liquid phase standard state.

Bulk Electrostatics Formalism:

In an electrostatic theory of non-conducting media, the relative permittivity, ε of the medium was a scalar constant for isotropic homogeneous media and a scalar function of position for isotropic non-homogeneous media. The scalar electric potential Φ in a linear homogeneous medium as per the Poisson's equation was given by;

$$\varepsilon \nabla^2 \Phi = -4 \pi \rho f \quad (5)$$

For a linear isotropic non-homogeneous medium, nonhomogeneous Poisson equation was given by:

$$\nabla . (\varepsilon \nabla \Phi) = -4 \pi \rho f \quad (6)$$

Where ρf was the free charge density of the solute. Electric potential due to the polarized dielectric continuum and the polarization of the solute was called the reaction field ϕ, which was equal to the total potential Φ minus the electrostatic potential Φ(0) of the gas phase molecule. From this reaction field, we could calculate the free energy change due to the solvation process. If solute was considered rigid, the electrostatic free energy of solvation was given by:

$$\Delta G_{EP} = \langle \psi | H^{(0)} - e/2\, \varphi | \psi \rangle + e/2\, \Sigma_k\, Z_k\, \varphi_k - \langle \psi^{(0)} | H^{(0)} | \psi^{(0)} \rangle \quad (7)$$

Where e was the atomic unit of charge, φk was the reaction field calculated at atom k, Z_k was the atomic number of atom k, $H^{(0)}$ and $\psi^{(0)}$ were solute Hamiltonian function and electronic wave function in the gas phase. In the SMD model, the solvent accessible surface (SAS) was formed by the boundary which surrounds the nuclear-centered spheres of radii

ρk where the value of the radii depends on upon the atomic number of the atoms. The reaction field at any position r within the cavity was given by:

$$\phi\,(r) = \Sigma_m \frac{q_m}{|r - r_m|} \tag{8}$$

where r_m was the position of an element m of surface area on the solute- solvent boundary and q_m were the apparent surface charge on element m.

Cavity-Dispersion-Solvent- Structure Formalism:

The free energy of solvation partitioned section in equation (1) G_{CDS} was given by:

$$G_{CDS} = \Sigma_k^{atoms}\, \sigma_k\, A_k(R, \{R_{Z_k} + r_s\}) + \sigma^{[M]}\, \Sigma^{atoms}_k\, A_k\,(R, \{R_{Z_k} + r_s\}) \tag{9}$$

Where σ_k and $\sigma^{[M]}$ were the atomic surface tension of atom k and the molecular surface tension respectively and A_k was the solvent-accessible surface area (SASA) of atom k. $R\{R_{Z_k} + r_s\}$ was the geometry with the set R_{Z_k} of all atomic van der waal radii and the solvent radius rs added to the van der Waal radii of atom.

The atomic surface tension was evaluated using following equation:

$$\sigma_k = \sigma_{Z_k} + \Sigma^{atoms}_k\, \sigma_{Z_k Z_k} T_k\,(\{Z_{k'}, R_{kk'}\}) \tag{10}$$

where σ_{Z_k} was an atomic number specific parameter, $\sigma_{Z_k Z_k}$ was the parameter that depends on atomic number of atoms k and k' and T_k $(\{Z_{k'}, R_{kk'}\}$ was a geometry dependent function called cutoff tanh. The above two formalisms when summed together, gave the free energy of solvation at standard state.

Chapter 2[1]: Reactivity of hydroxyl radicals with dissolved organic matter in the aqueous phase advanced oxidation processes

2.1. Abstract

Advanced Oxidation Processes (AOPs) that produce highly reactive hydroxyl radicals (HO•) destroy synthetic organic chemicals in water and wastewater treatment processes. The presence of background dissolved organic matter (DOM) is detrimental to the overall performance of AOPs. While overall reactivity of HO• with surrogate DOM has been extensively studied, little is known about the molecular-level interaction and reactivity of HO• with DOM. In this study, we use quantum mechanics-based computational chemistry techniques to study the molecular-level reactivity of HO• with a widely accepted model monomer of Suwanee River Fulvic Acid NOM, Temple Northeastern Birmingham (TNB) model. We calculate the aqueous-phase free energies of activation and van der Waals (vdW) interaction to examine the HO• reactivity and accessibility of all the possible reactive sites of the TNB model, respectively. We further compare the reactivity and accessibility to those that are calculated based on the segmented TNB model. These comparisons reveal that the surrounding functional group(s) significantly affects the HO• reactivity with the specific site of the TNB model by reducing the aqueous-phase free energies of activation. This is the first study to investigate the molecular-level reactivity and interaction of HO• with a model monomer of surrogate DOM. The results provide mechanistic insights into the local reactivity of HO• and the initial fate of DOM transformation.

[1] Chapter 2 is prepared as a manuscript and will be submitted to the Environmental Science & Technology journal.

2.2. Introduction

A wide variety of synthetic organic chemicals such as pharmaceuticals, personal care products, endocrine disrupting chemicals, pesticides, and herbicides are in use and production. The conventional water and wastewater treatment processes are found to be ineffective in removing these organic chemicals. (Amin et al., 2014). Accordingly, very low levels of these chemicals in the range from micro to nanogram have been reported in environmental waters. (Snyder et al., 2003). Accordingly, the presence of low levels of chemicals raises significant public concern about water.

Advanced Oxidation Processes (AOPs) are attractive and promising treatment technologies that can destroy the low level of organic chemicals. AOPs generate highly reactive electrophile hydroxyl radicals (HO•), at atmospheric pressure and ambient temperature. The HO• reacts with electron rich sites of organic compounds and initiates complex chain reactions. Because of the non-selectivity of HO•, the presence of background dissolved organic matter (DOM) significantly affects the performance of AOPs by scavenging HO•.

DOM is a heterogeneous surrogate organics containing both hydrophilic and hydrophobic components with different functional groups, sizes, and reactivity. (Weng et al., 2012). Leenheer 2007, in his paper, summarized an overview of the different model structures approximated till the time that would help to develop molecular structures of NOM. Six specific models were derived from the model approximations of Suwannee River Fulvic Acid obtained from International Humic Substances Society. DOM was fractionated from water available from various surface and ground water bodies. The reactivity of DOM with water treatment processes was analyzed by Leenheer J.A. in 2004.

Figure 3 shows TNB model representing the average humic substance molecule with a chemical composition $C_{38}H_{39}O_{16}N_2$ and a molecular weight of 753 g/mol.

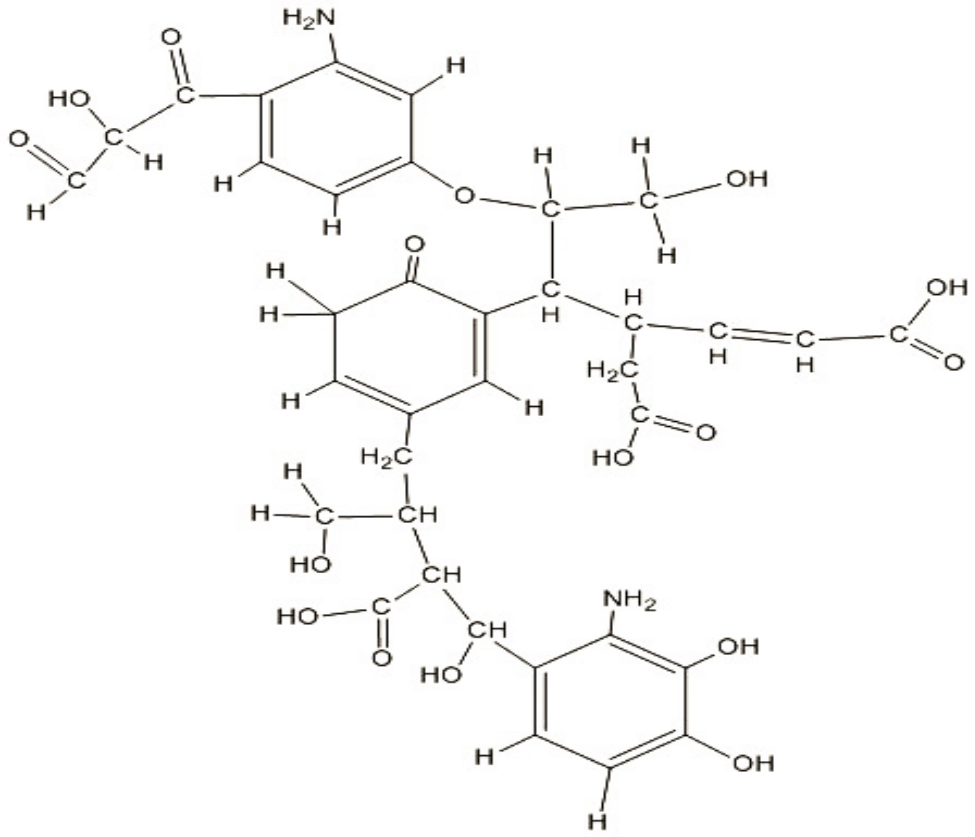

Figure 3: Temple Northeastern Birmingham Model

The selection of the TNB model for this study was based on the study by Sein et al., 1999 that stated: "TNB is a universal average formula unit of humic acids". Also, as per the theoretical study on fulvic acid structures by Alvarez-Puebla et al., 2006, "the TNB model of humic acid has some properties similar to fulvic acids like solubility and electronic and

vibrational spectra". TNB model was the simplest structure with a variety of functional groups attached to it which provided scope for a diverse study for the reactivity with HO•.

Although many experimental studies have been conducted on the overall reactivity of HO• (i.e., scavenging) with surrogate DOM by measuring the second-order reaction rate constants with various DOM, molecular-level HO• reactivity, and interaction with DOM are not well understood. For example, Westerhoff et al., 2007 reported the second-order reaction rate constants with various DOM and their isolates in the range from (1.39±0.16) $x10^8$ $M^{-1}s^{-1}$ to (4.53±0.54) $x10^8$ $M^{-1}s^{-1}$. McKay et al., 2011 reported the temperature dependent second order reaction rate constants with NOM including Suwannee River Fulvic Acid and Elliot Soil Humic Acid and effluent organic matter from wastewater treatment processes. Their studies determined the Arrhenius activation energies and frequency factors ranging from 2.56 to 7.15 kcal/mol and from (1.21±0.09) $x10^8$ to (9.37±0.07) x 10^8 $M^{-1}s^{-1}$, respectively. Rosario-Ortiz et al., 2008 also reported the hydroxyl radical rate constants with non-isolated effluent organic matter ranging from (0.27±0.01) $x10^9$ to (1.21±0.17) $x10^9$ $M^{-1}s^{-1}$. While these reaction rate constants indicate the overall reactivity with various DOM, it is not understood how HO• approach the potential reactive sites of DOM and how different each HO• reactivity with the associated reactive sites.

These elementary level reactions of HO• with the individual reactive site of DOM molecule can be understood and modeled with the help of computer-based modeling using computational chemistry. It provides a platform to develop new molecular structures or to model reactions and obtain parameters such as transition state structures or transition state energies which are hard to obtain experimentally. Also, it helps to develop an ideal

situation under which a reaction would occur. These ideal situations are a good reference any experimental investigations are planned to perform.

Computational chemistry is applied to two streams namely classical mechanics and quantum mechanics. Quantum mechanical methods are classified into *ab initio* or semi-empirical methods.

Ab-initio methods are those robust quantum mechanical methods that do not incorporate any empirical parameters in their calculations and equations utilized are completely based on the theoretical principles of quantum theory.

In this study, we use quantum mechanical calculations to understand the molecular-level reactivity and interactions of HO• with a model monomer of SRFA, TNB model. First, we first optimize the TNB structure at the lowest energy point. Then, we calculate the aqueous-phase free energies of activation and vdW-interactions of HO• with all the possible reactive sites of the TNB model, respectively. We also compare these free energies to those that are obtained based on the segmented TNB models.

2.3. Materials and Methods

These theoretical investigations of reactivity of HO• with TNB model were performed with Gaussian09 revision D.02 provided by Michigan Tech high-performance cluster "Superior" and also with the workstation established by Dr. Daisuke Minakata.

As we discussed and determined from the comparison of various quantum mechanical methods and basis sets in Supporting Information, we calculated the both gaseous- and aqueous-phase free energies of activation and interaction at the level of

B3LYP/3-21+G*, and M06-2X/cc-pVDZ quantum mechanical methods. (Riley et al., 2007).

We used our own N-layered integrated molecular orbital and molecular mechanics (ONIOM) to determine the active layer for the reaction in the study. (Vreven T. et al., 2003).It is a technique used to model large molecules by defining them under different layers such as active layer, medium layer and a lower layer. Each of these layers is optimized using different quantum mechanical methods starting from a computationally expensive method for an active layer to least expensive method for the lower layer. The active layer of the molecule was determined based on the site chosen for the reaction. It is the smallest layer of the molecule where bond formation or breaking takes place and optimization of the active layer are performed with an accurate and computationally expensive method. The active layer was chosen such that functional groups attached nearby a specific site of the molecule gets involved in the segment chosen for reaction study. The molecule was defined by two layers, higher and lower layer. The higher layer was optimized using quantum mechanical DFT method at the level of B3LYP/3-21+G* and the lower layer was optimized using PM3 semi-empirical method. (Vreven T. et al., 2006). We determined five different active layers by selecting the segments of the TNB model based on the availability of the functional group around a particular site of the molecule The Berny's optimization algorithm was used for the geometrical optimization of the structure. This algorithm utilizes the forces on the atoms and the Hessian matrix to produce a local minimum on the potential energy surface of an optimized molecule. When ONIOM is used to define the layers of the molecule this energy calculation can be defined in two

ways for two layered molecules and for three layered molecules. For a two layer ONIOM model, molecular energy is defined as follows:

$$E^{high}(R) \approx E^{low}(SM)+\{E^{low}(R)-E^{low}(SM)\}+\{E^{high}(SM)-E^{low}(SM) \quad (11)$$

Here high and low means the active layer and the lower layer respectively. SM denotes a small model or segment and R denotes the real system or whole molecule. This equation can also be reduced to the form:

$$E^{ONIOM} = E^{low}(R) + E^{high}(SM) - E^{low}(SM) \quad (12)$$

Similarly, for a three layered ONIOM model, the energy is defined as follows:

$$E^{high}(R) \approx E^{ONIOM} = E^{low}(R) + E^{medium}(IM) + E^{high}(SM) - E^{low}(IM) - E^{medium}(SM) \quad (13)$$

Where symbols have their usual meanings. For the hydroxyl radical ground state in both gaseous and aqueous phases, the structure and free energy were calculated at the level of B3LYP/3-21+G*, and M06-2X/cc-pVDZ. The SMD solvation model by Marenich A.V. et al., 2009 was used to determine the optimized structure and frequency.

For the van-derWaal-interaction structures were also optimized at the level of B3LYP/3-21+G*, and M06-2X/cc-pVDZ quantum mechanical methods and PM3 semi-empirical method and their frequencies were calculated at this level of theory and the molecule was defined under ONIOM.

For the transition structure, the QST 3 method was used to find the local transition states because it is impractical to attempt to find true saddle points and transition states for the fast HO• reaction. (Dash et al., 2012). All of the transition states was verified with the

imaginary frequency and the IRC analysis was performed to confirm the connectivity among reactant, transition state, and product for several representative transition states. The gaseous phase transition states were optimized first and frequency was calculated. Then, the aqueous phase transition states were optimized based on the optimized gaseous-phase structure using the SMD solvation model. In order to calculate the free energy of activation and vdW-interaction, equations were used:

$$\Delta G^{act}{}_{aq,calc} = \Delta G^{TS}{}_{aq,calc} - \Delta G^{reacctants}{}_{aq,calc} \quad (14)$$

$$\Delta G^{interaction}{}_{aq,calc} = \Delta G^{vdW\ complex}{}_{aq,calc} - \Delta G^{reactants}{}_{aq,calc} \quad (15)$$

The TNB model was segmented into 7 different parts in order to compare the calculated free energies of activation and interactions with those that are obtained from the overall TNB molecule. The segmented TNB structures were optimized and the frequency were calculated at the level of both B3LYP/3-21+G* and M06-2X/cc-pVDZ method.

2.4. Results and Discussions

For the main study, we chose the lowest energy conformer of TNB model with SRRSRRS conformation and the single point energy of -9785.73 kcal/mol determined by semi-empirical PM3 method as reported. (Sein et al., 1999). We investigated the reactivity of HO• at different sites of this TNB model namely aliphatic carbons, alkenes, aromatic rings. We modeled the reaction mechanisms such as H-atom abstraction, HO• addition to the aromatic ring, and HO• addition to alkenes.

For this at first, the minimum energy ground state optimized structures of TNB and HO• were obtained in both gas and aqueous phase and were defined under ONIOM as shown in

figure 4 below. In addition to this, various sites of the TNB model on which the reactions with HO• was performed are summarized in figure 5 below.

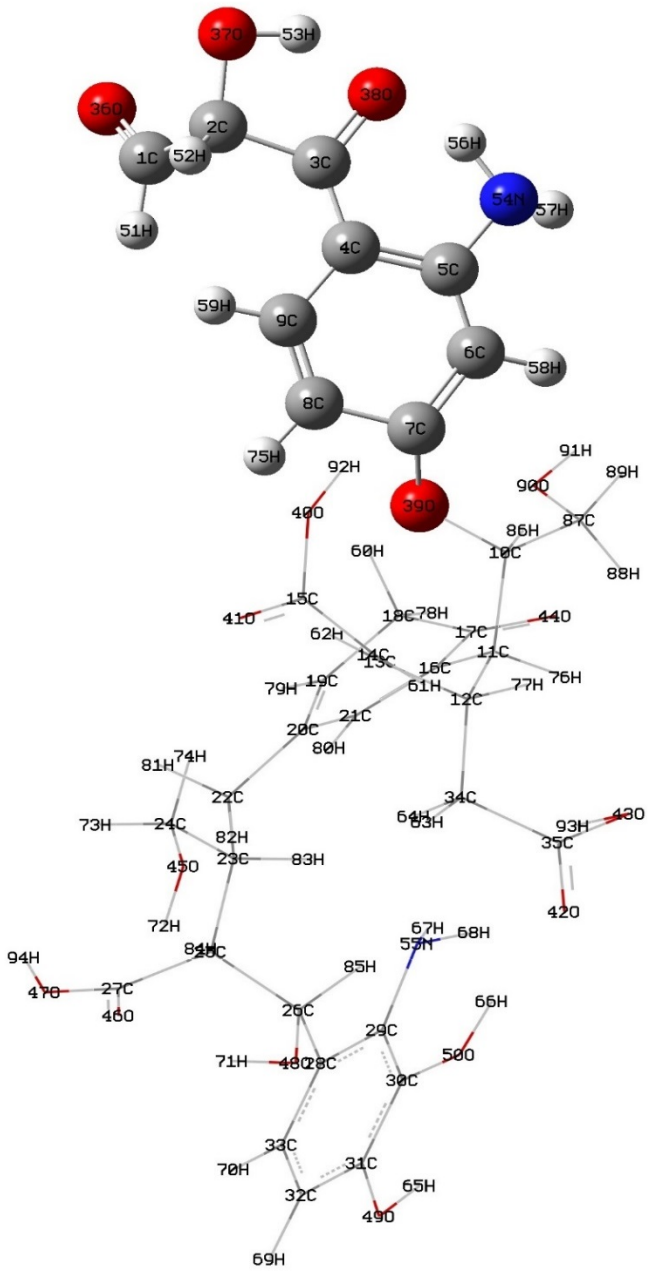

Figure 4(a): Optimized gas phase TNB with 5 different active layers (a) Active layer 1

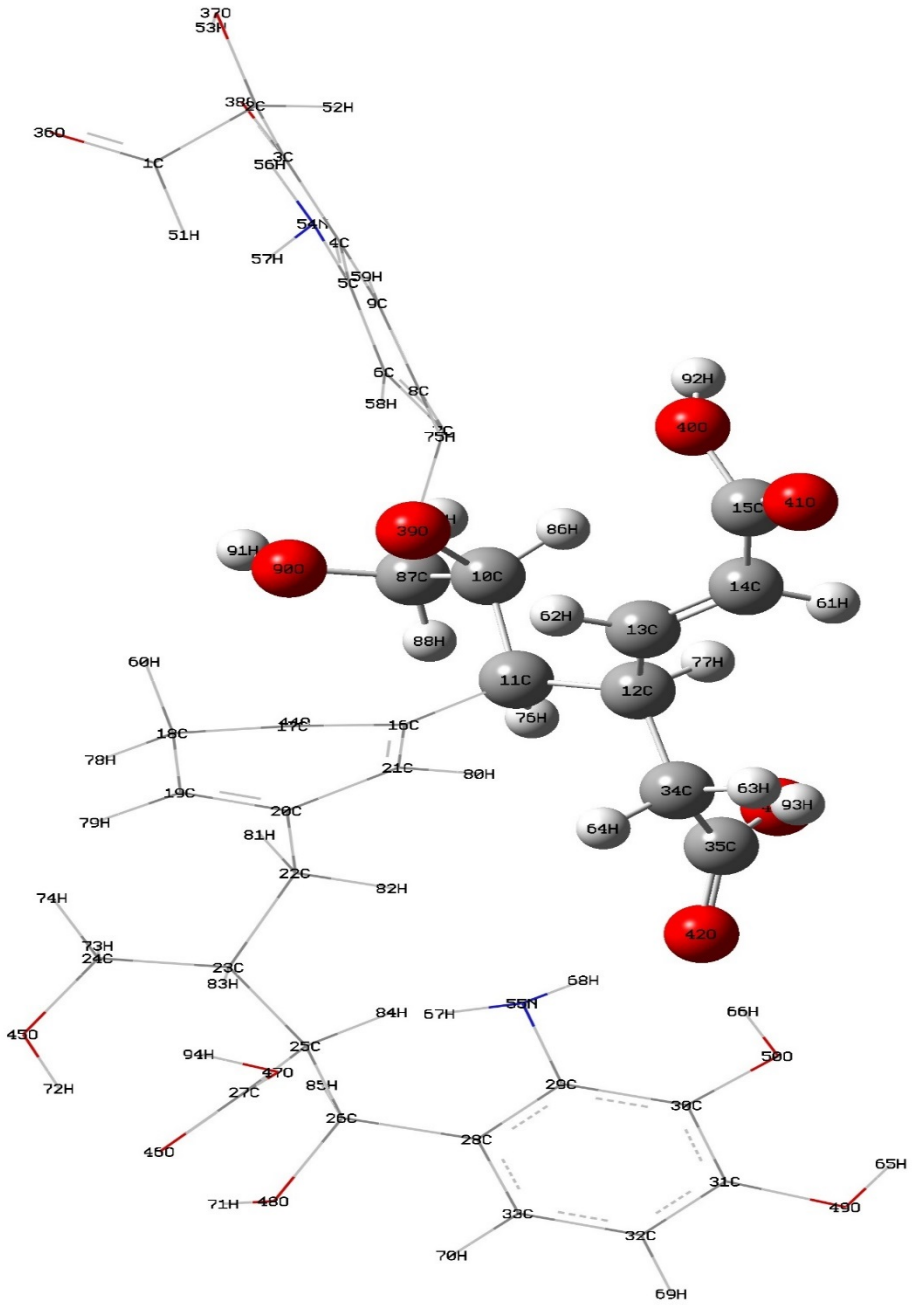

Figure 4(b): Optimized gas phase TNB with (b) Active layer 2

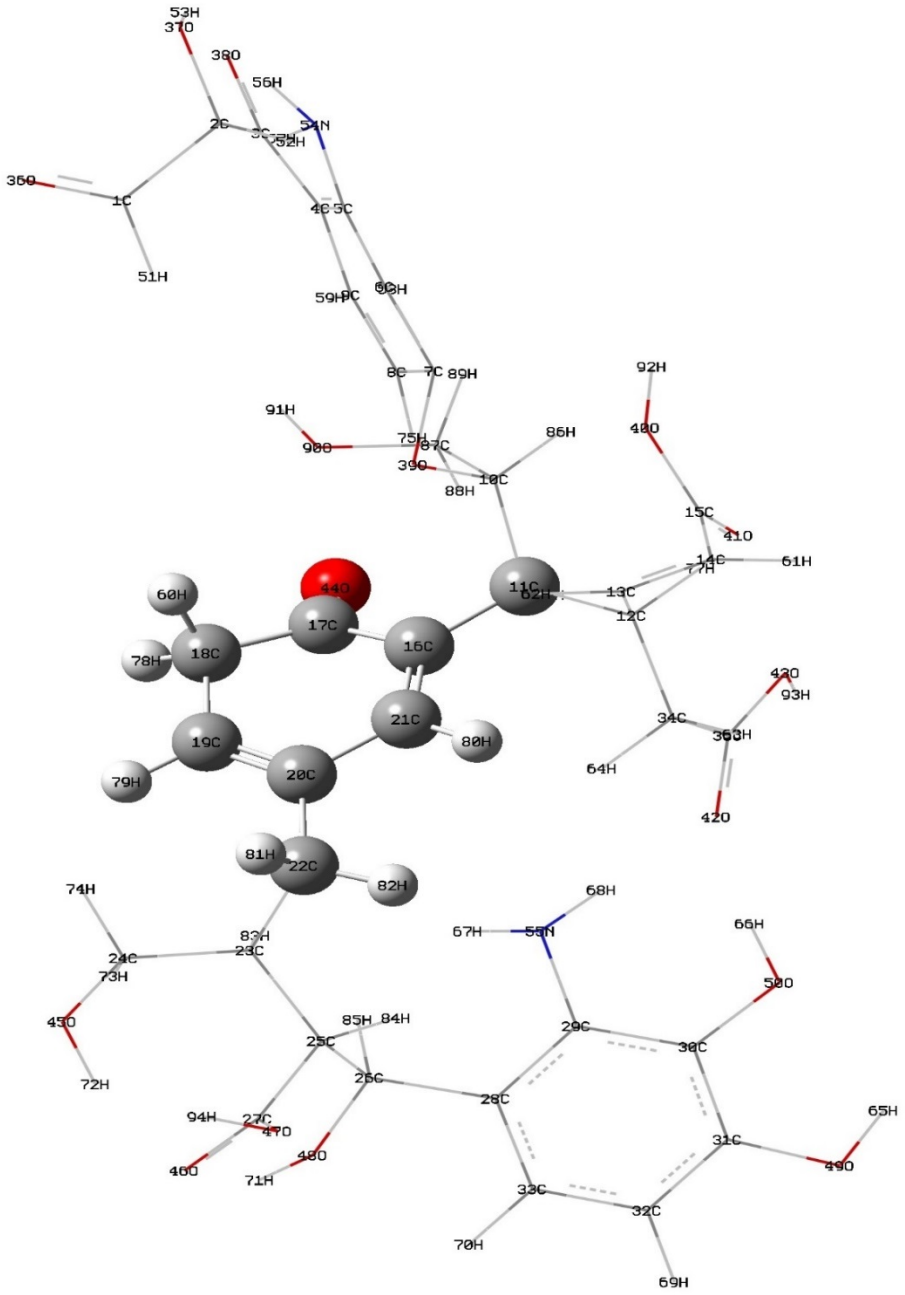

Figure 4(c): Optimized gas phase TNB with (c) Active layer 3

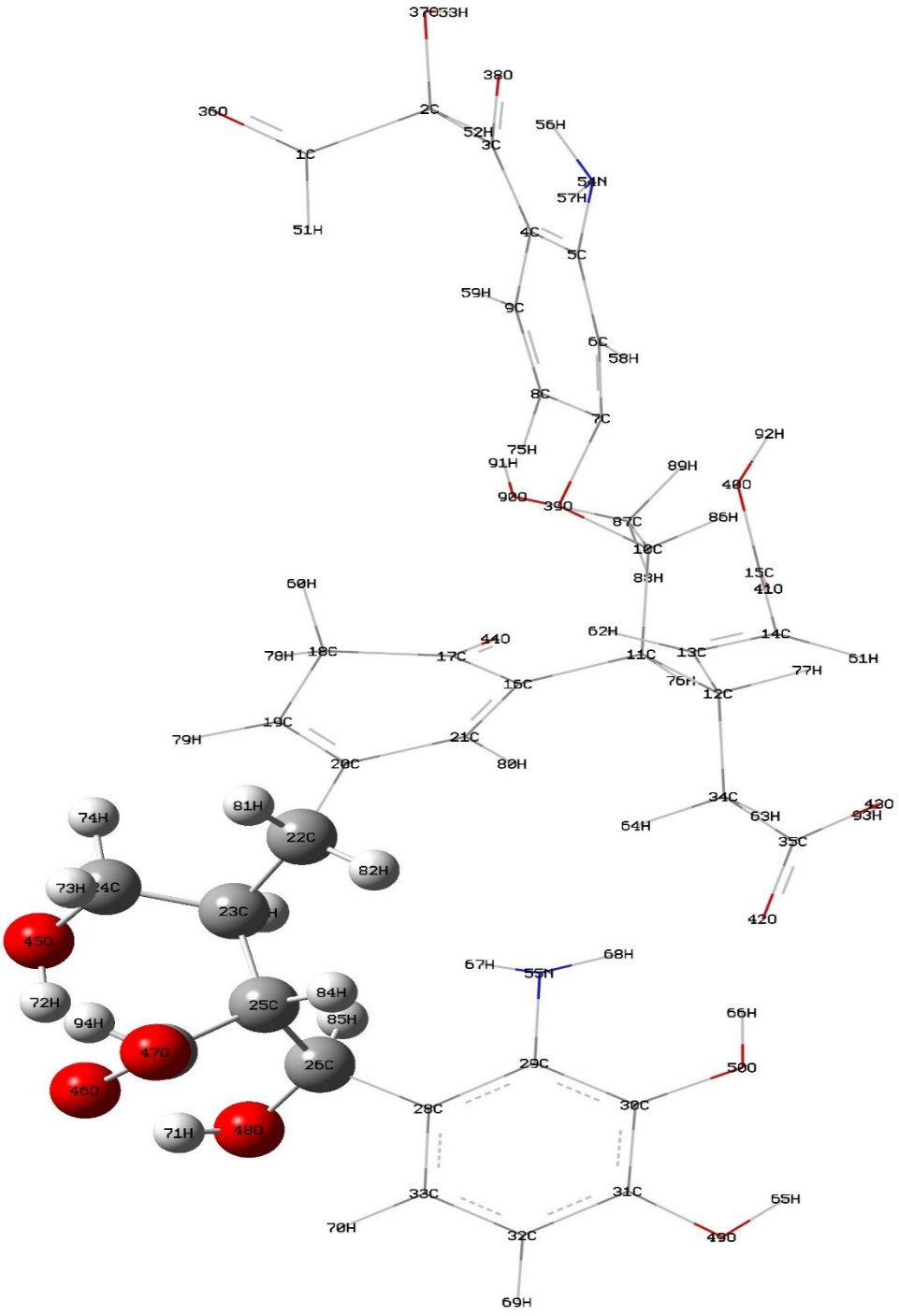

Figure 4(d): Optimized gas phase TNB with (d) Active layer 4

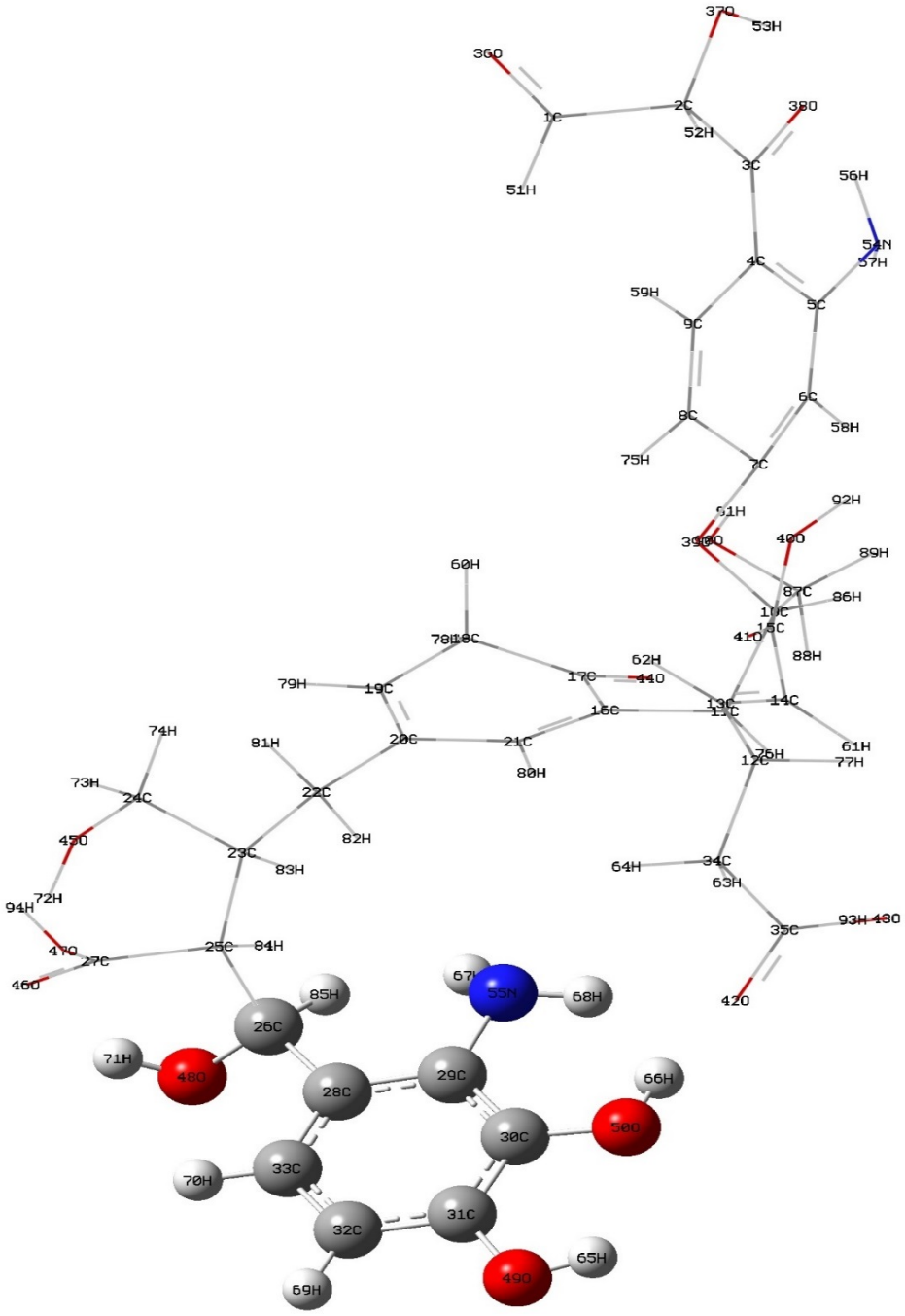

Figure 4(e): Optimized gas phase TNB with (e) Active layer 5.

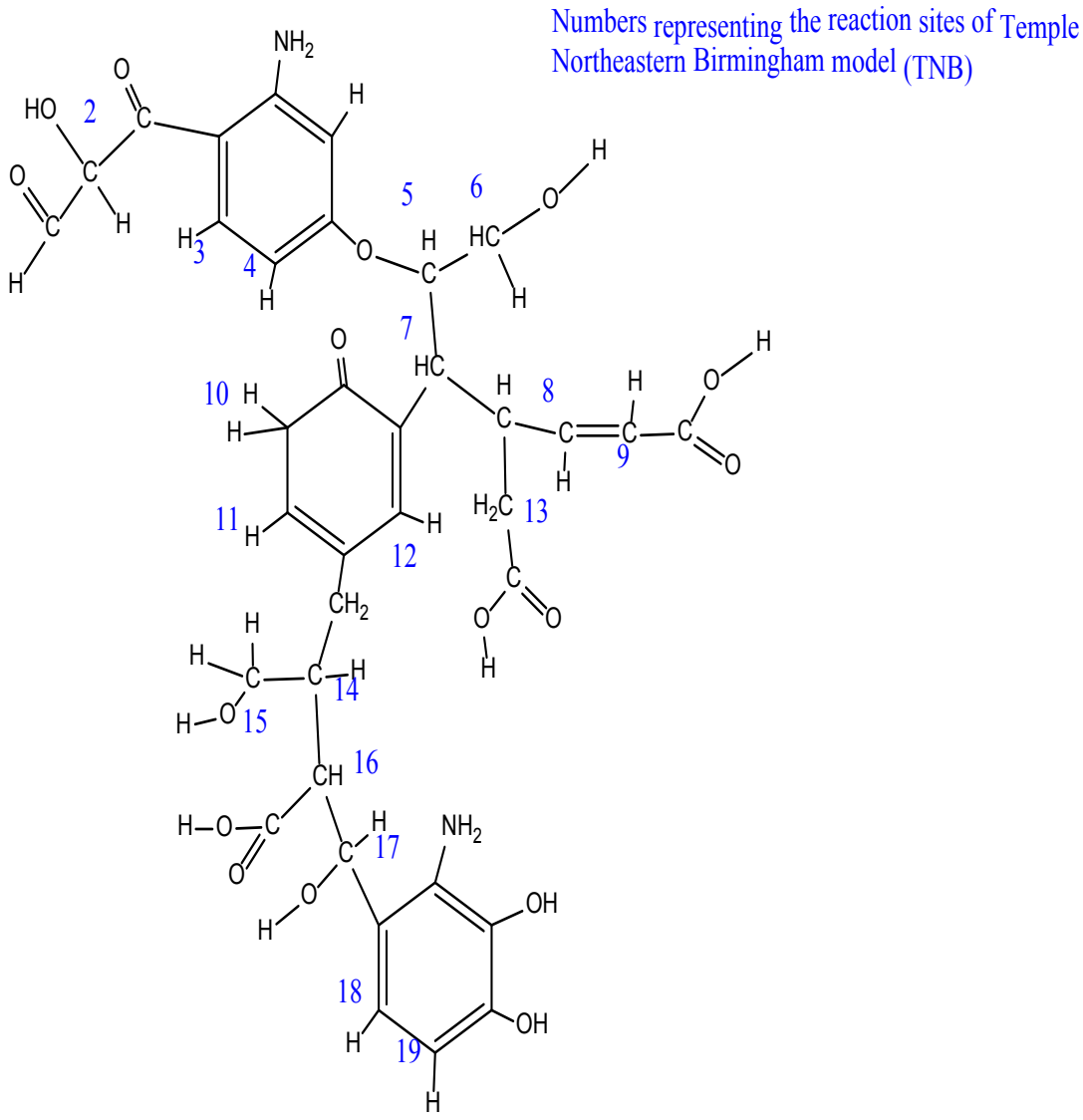

Figure 5: TNB model showing various reactive sites for reactions with HO•.

There was a total of 19 potential sites that HO• attack including 8 for HO• addition to an unsaturated carbon of aromatic ring and alkenes of the TNB model, 9 for H-atom abstraction from a C-H bond, and 2 for HO• interaction with amine nitrogen via electron transfer. It turns out that the gaseous-phase free energies of activation are in the range from

-2.12 kcal/mol to -31.63 kcal/mol based on the calculated 19 sites. For HO• addition to aromatic ring at site 11 the minimum free energy of activation was observed. The site 11 was surrounded and influenced by two OH and one NH2 functional group. The maximum free energy of activation was observed for H-atom abstraction at site 15. Site 15 was comparatively less influenced by functional groups. One of the obtained gaseous phase transition state optimized structures is shown below in figure 6.

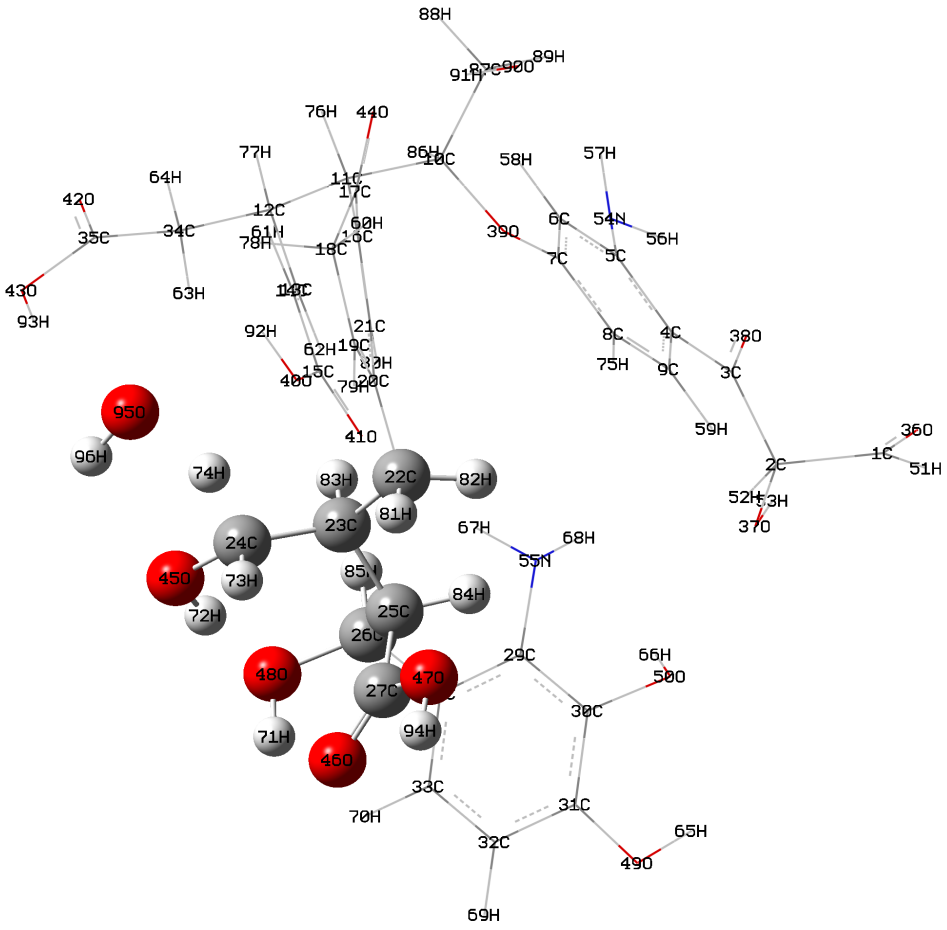

Figure 6: Optimized transition state structure of H atom abstraction from site 15 of the TNB molecule.

For the aqueous-phase, the calculated free energies of activation range from -4.20 kcal/mol to -27.20 kcal/mol based on the calculated 9 points. The highest and lowest free energy of activation was obtained as -4.22 kcal/mole at site 18 for HO• addition to the aromatic ring and -27.20 kcal/mol at site 11 for HO• addition to aromatic ring respectively. Site 18 was only under the slight influence of COOH functional group, however, Site 11 in the aqueous phase was surrounded by 2 OH and one NH_2 functional group.

From the overall observation, the lowest aqueous-phase free energy of activation was -27.20 kcal/mol for HO• addition to the aromatic ring on site 11. HO• addition to alkenes at site 8 was found to be the second most reactive site with -25.45 kcal/mol of aqueous-phase free energy of activation. In contrast, the site 18 was observed to be the least reactive site with -4.42 kcal/mol of free energy of activation for HO• addition to an aromatic ring.

All the calculated free energies of activation at various sites of the TNB model obtained in gaseous and the aqueous phase is summarized in figure 7 below.

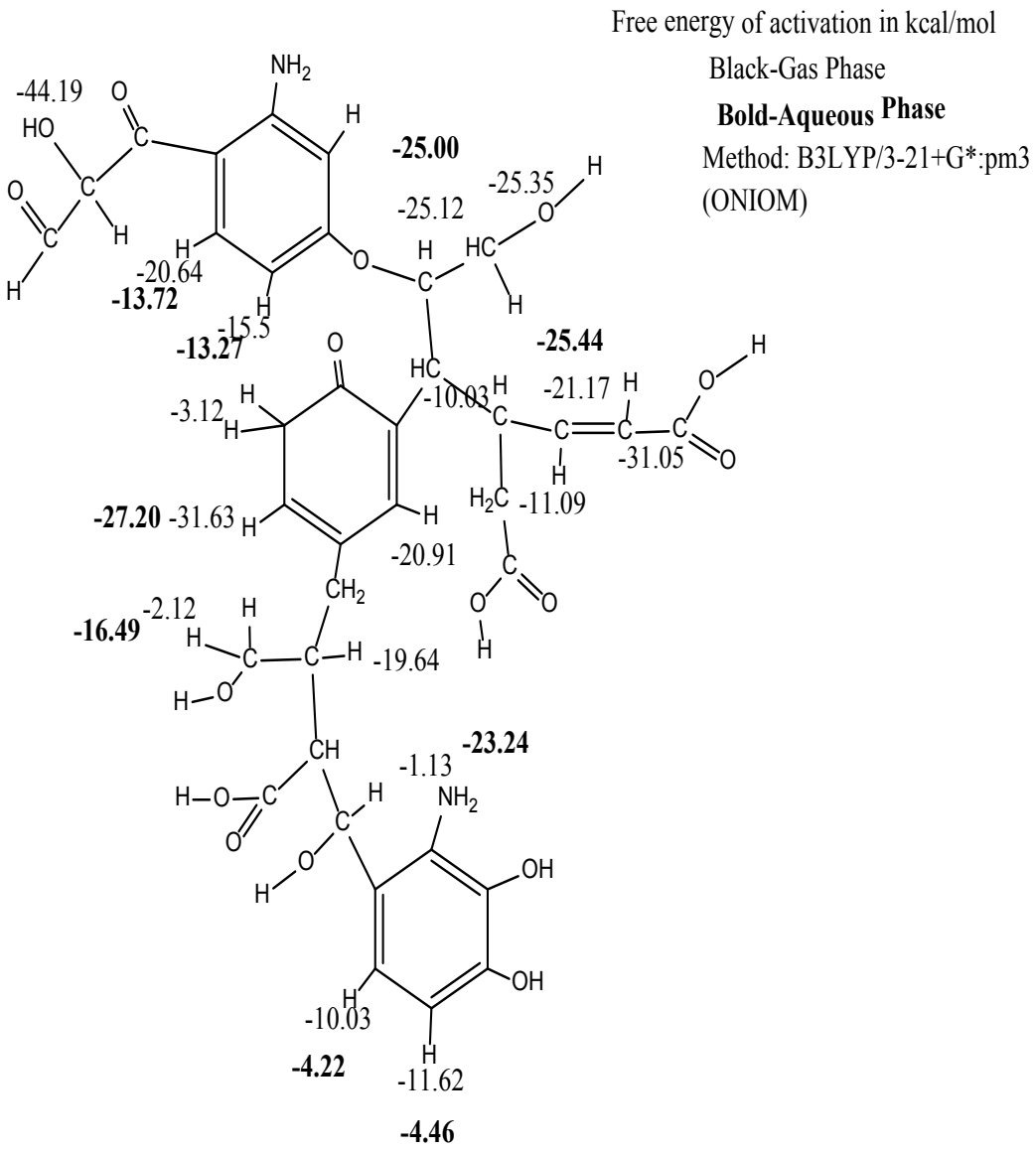

Figure 7: TNB structure summarizing the obtained free energy of activation in gas and the aqueous phase in kcal/mol.

In order to evaluate how neighboring functional groups affect the aqueous-phase free energies of activation, we segmented the TNB model into 7 parts and compared the free energies to those that were obtained based on the overall TNB structure. Figure 8 represents how the entire TNB was segmented into 7 parts.

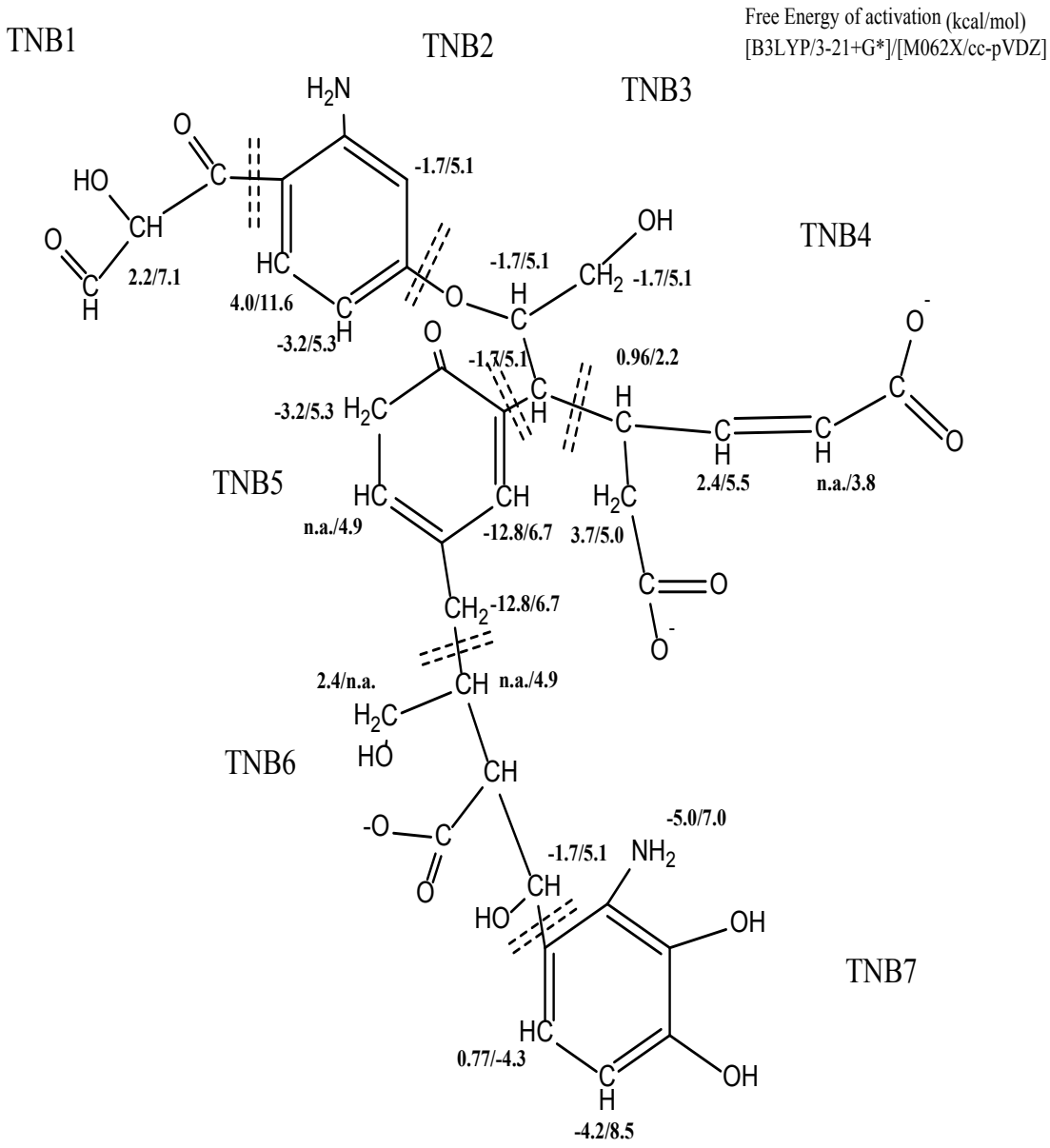

Figure 8: Aqueous phase TNB structure with the segments showing the free energy of activation evaluated at various sites using the two methods.

In figure 8, the segmented molecule results are shown in the aqueous phase at the level of B3LYP/3-21+G* and also at the level of M062X/cc-pVDZ. The maximum aqueous-phase free energy of activation of 4 kcal/mol was obtained at site 3 on segment TNB2 and minimum -12.8 kcal/mol at site 12 on segment TNB5. Similarly, at segment TNB3 site 5,

the free energy of activation obtained was -1.7 kcal/mol and at site 18 of segment TNB7, the free energy of activation was recorded as 0.77 kcal/mol.

Comparison between the segmented and overall TNB molecule on obtained aqueous phase free energy of activation is summarized in table 1 below:

Table 1: Comparison between the segmented and overall TNB molecule summarizing the effect of nearby functional groups on the free energy of activation at its various sites.

Free energy of activation	**Overall Molecule**	**Segmented Molecule**
Maximum free energy of activation.	-4.22 kcal/mol at site 18. Influenced only by 1 COOH functional group.	4 kcal/mol at segment 2 site 3. No functional group influence nearby the site.
Minimum free energy of activation.	-27.20 kcal/mol at site 11. Influenced by 2 OH and 1 NH_2 functional groups.	-12.8 kcal/mol segment 5 site 12.
Free energy of activation at site 18.	Negative value (-4.42 kcal/mol) due to the presence of COOH functional group (low).	Positive value (0.77 kcal/mol) due to no influence by any functional group.
Free energy of activation at site 5.	-25 kcal/mol Influenced by the COOH and OH functional groups	-1.7 kcal/mol Influenced by only one OH functional group.

With this discussion and comparison, we could interpret that effect of the presence of a number of functional groups in the vicinity of the HO• reaction with DOM, actually enhances the HO• reactivity with DOM by lowering the free energy of activation values

when the whole molecule was considered. It could be seen that the free energy of activation values decreased in the whole molecule when segmented and the whole molecule was compared.

In addition to this, aqueous-phase free energies of interaction was calculated and the HO• accessibility on the possible reactive sites of the overall TNB molecule was compared with the segmented TNB molecule. Figure 9 and figure 10 below summarizes the free energy of interaction calculated at various sites of the overall and segmented TNB molecule respectively.

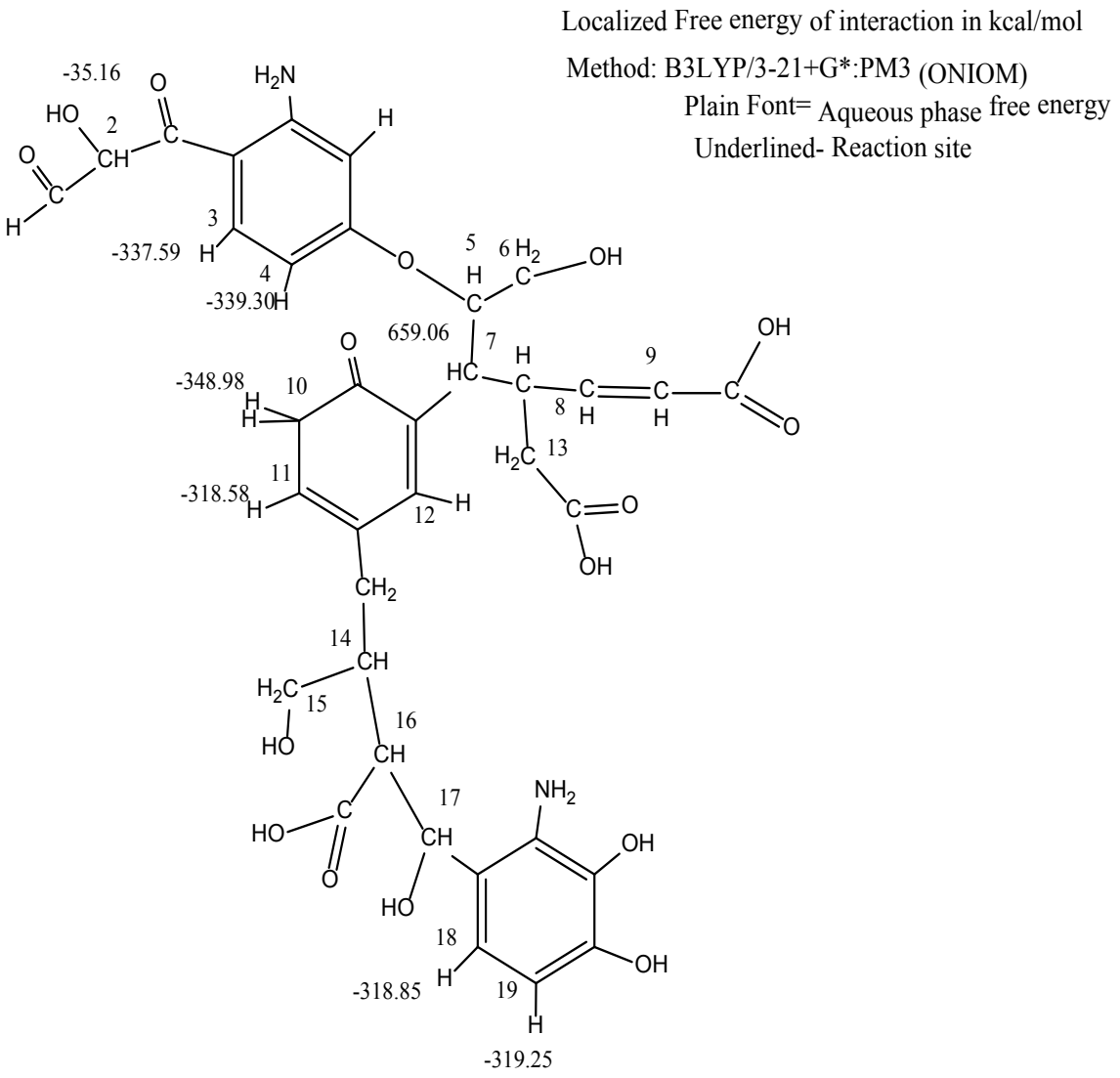

Figure 9: Localized free energy of interaction in the aqueous phase in kcal/mol for the overall TNB molecule.

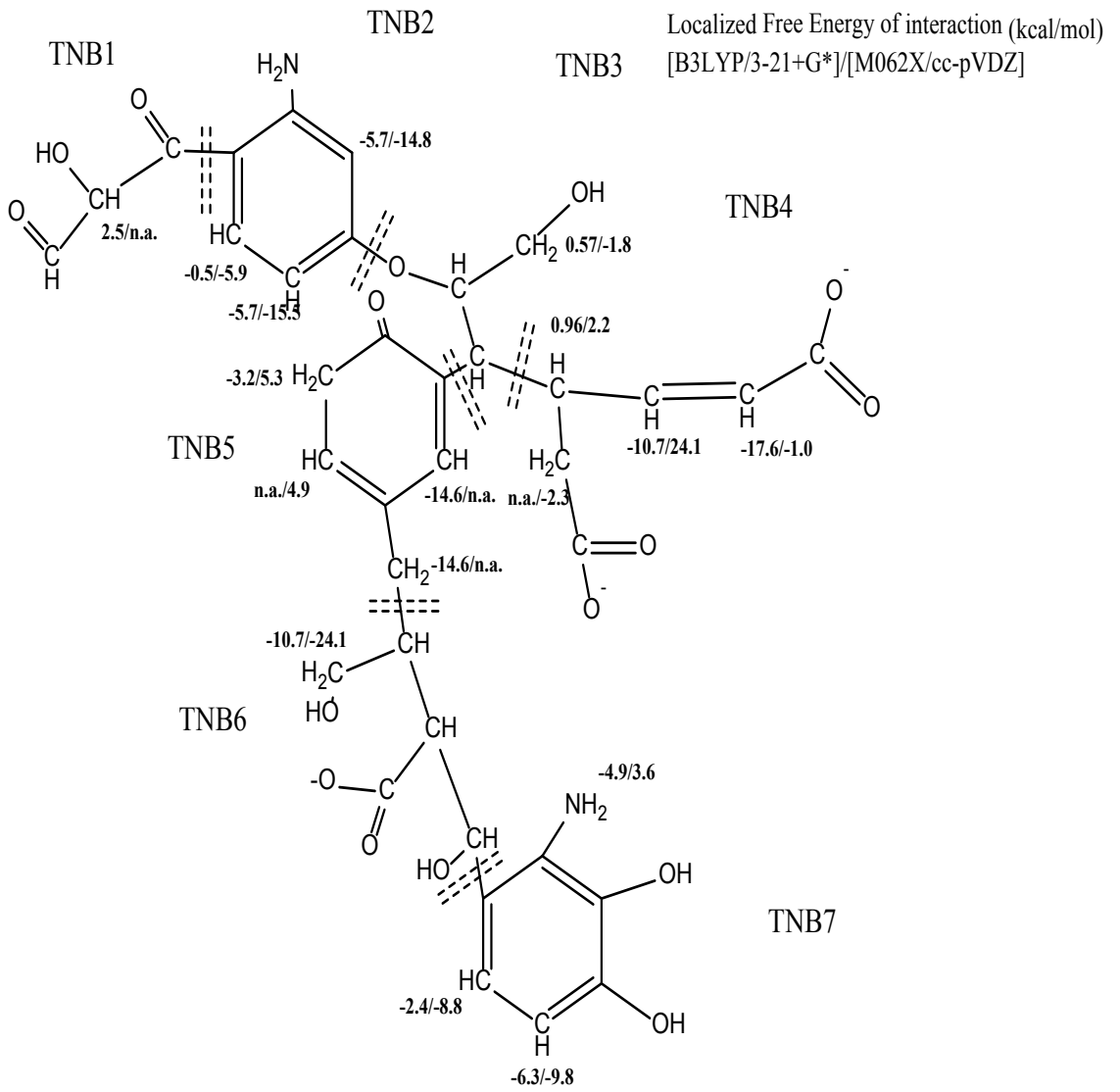

Figure 10: Aqueous phase localized free energy of interaction in kcal/mol for different segments of TNB

The aqueous phase localized van der Waal free energy of interaction was evaluated at 8 different sites of the overall TNB molecule. The maximum interaction energy obtained was 659.06 kcal/mole at site 7. The minimum localized van der Waal interaction energy was observed to be -348.98 kcal/mole for site 10 that corresponds to H-atom abstraction

reaction. Site 10 was free and not surrounded by any aliphatic branches or functional group when compared to site 5, 7 or 8.

Table 2 below summarizes the comparison and discussions between the segmented and overall TNB molecule on obtained aqueous phase localized free energy of interaction.

Table 2: Comparison between the segmented and overall TNB molecule summarizing the effect of nearby functional groups on localized free energy of interaction at its various sites.

Interaction site	**Overall Molecule**	**Segmented Molecule**
Maximum free energy of interaction on site 2.	-35.16 kcal/mol	2.5 kcal/mol
Free energy of interaction at site 18.	-318.85 kcal/mol The site was influenced by 2 COOH and 1 OH functional groups.	-2.4 kcal/mol No significant influence of functional group observed.
Minimum free energy of interaction at site 10.	-348.98 kcal/mol	-17.6 kcal/mol
Free energy of interaction at site 3.	-337.59 kcal/mol The site was influenced by a COOH, OH and a ketone functional group.	-0.5 kcal/mol The individual segment was not influenced by any functional group.
Free energy of interaction at site 4.	-339.30 kcal/mol The site was influenced by 2 COOH functional groups.	-5.7 kcal/mol The individual segment was not influenced by any functional group.

2.5. Conclusion

This is the first study that illustrates about the different molecular reactions that a dissolved organic matter undergoes at its various sites with HO•. From the outcomes of this analysis it was interpreted that the neighboring functional groups significantly affect the reaction by enhancing the reactivity and reducing the energy barrier or free energy of activation. Greater the number of functional group influencing the site of reaction, lower was the free energy of activation observed as discussed in table 1. This implies that lower free energy of activation leads to reduced energy barrier. The reaction will proceed relatively faster due to lowered energy barrier and will increase the reaction rate constant based on the Arrhenius equation used in reference to the transition state theory.

Future Work

This study is the first step towards investigation of the molecular level reactivity and interaction of HO• with a model monomer of surrogate DOM. The outcome of this study provides a mechanistic insight into the localized reactivity of HO• and initial DOM transformation. However, future studies could aim at analyzing the overall reactivity.

In addition to the free energy of activation and interaction in aqueous phase, the effect of solvation is yet to be explored. Researchers can also focus on understanding the dynamics of the influence of water molecules on these molecular level reactions between HO• and TNB molecule.

This study was focused on the lowest energy conformer of model monomer of fulvic acid. In future, the molecular level reactivity can be studied for other large sized model of dissolved organic matter.

The free energy of activation and free energy of interaction at various sites of the TNB model in this study have been evaluated using computationally less demanding quantum mechanical methods due to the available time and scratch space. Researchers can perform this study using more accurate and computationally expensive quantum mechanical methods such as M062X, Moller-Plesset perturbation theory or Coupled Cluster method.

References

Crittenden J.C., Trussell R.R., Hand D.W., Howe K.J. and Tchobanoglous G. (2012) MHW Water Treatment Principles and Design, Hoboken NJ: John Wiley & Sons.

Ritson, J.P., Graham N.J.D., Templeton M.R., Clark J.M., Gough R., Freeman C. (2014) The Impact of Climate Change on the Treatability of Dissolved Organic Matter (DOM) in Upland Water Supplies: A UK Perspective, *Science of the Total Environment* 473-474: 714-30.

Minakata, D., Li K., Westerhoff P., and Crittenden J.C. (2009) Development of a Group Contribution Method to Predict Aqueous Phase Hydroxyl Radical (HO•) Reaction Rate Constants, *Environmental Science & Technology* 43.16: 6220-227.

Westerhoff P., Mezyk S.P., Cooper W.J. and Minakata D. (2007) Electron Pulse Radiolysis Determination of Hydroxyl Radical Rate Constants with Suwannee River Fulvic Acid and Other Dissolved Organic Matter Isolates, *Environmental Science & Technology* 41.13: 4640-646.

Rosario-Ortiz F.L., Mezyk S.P., Doud D.F.R. and Snyder S.A. (2008) Quantitative Correlation of Absolute Hydroxyl Radical Rate Constants with Non-Isolated Effluent Organic Matter Bulk Properties in Water, *Environmental Science & Technology* 42.16: 5924-930.

Rosario-Ortiz F.L., Snyder S.A. and Suffet I. H. (Mel). (2007) Characterization of the Polarity of Natural Organic Matter under Ambient Conditions by the Polarity Rapid Assessment Method (PRAM), *Environmental Science & Technology* 41.14: 4895-900.

Rosario-Ortiz F.L., Snyder S.A. and Suffet I. H. (Mel). (2007) Characterization of Dissolved Organic Matter in Drinking Water Sources Impacted by Multiple Tributaries, *Water Research* 41.18: 4115-128.

Mckay, G., Dong M.M., Kleinman J., Mezyk S.P. and Rosario-Ortiz F.L. (2011) Temperature Dependence of the Reaction between the Hydroxyl Radical and Organic Matter, *Functions of Natural Organic Matter in Changing Environment*: 329-33.

Dong, M.M., Mezyk S.P. and Rosario-Ortiz F.L. (2010) Reactivity of Effluent Organic Matter (EfOM) with Hydroxyl Radical as a Function of Molecular Weight, *Environmental Science & Technology* 44.15: 5714-720.

Mckay G. and Rosario-Ortiz F.L. (2015) Temperature Dependence of the Photochemical Formation of Hydroxyl Radical from Dissolved Organic Matter, *Environmental Science & Technology* 49.7: 4147-154.

Satinder A. and Kiril H. (2013) Novel Solutions to Water Pollution, Ionizing Radiation Techniques to Determine Hydroxyl Radical Efficiencies of Organic Pollutant Mixtures in Treated Wastewaters, *ACS Symposium Series* 1123.

Leenheer. J.A (2007) Progression from Model Structures to Molecular Structures of Natural Organic Matter Components, *Annals of Environmental Science*, Vol 1, 57-68.

Sein L.T., Varnum J.M. and Jansen S.A. (1999) Conformational Modeling of a New Building Block of Humic Acid: Approaches to the Lowest Energy Conformer, *Environmental Science & Technology* 33.4: 546-52.

Minakata D. and Crittenden J.C. (2011) Linear Free Energy Relationships between Aqueous Phase Hydroxyl Radical Reaction Rate Constants and Free Energy of Activation." *Environmental Science & Technology* 45.8: 3479-486.

Minakata D., Mezyk S.P., Jones J.W, Daws B.R. and Crittenden J.C. (2014) Development of Linear Free Energy Relationships for Aqueous Phase Radical-Involved Chemical Reactions, *Environmental Science & Technology* 48.23: 13925-3932.

Minakata D., Song W., Mezyk S.P. and Cooper W.J. (2015) Experimental and Theoretical Studies on Aqueous-phase Reactivity of Hydroxyl Radicals with Multiple Carboxylated and Hydroxylated Benzene Compounds, *Phys. Chem. Chem. Phys.* 17.17: 11796-11812.

Marenich, A.V., Cramer C.J. and Truhlar D.J. (2009) Universal Solvation Model Based on Solute Electron Density and on a Continuum Model of the Solvent Defined by the Bulk Dielectric Constant and Atomic Surface Tensions, *The Journal of Physical Chemistry B J. Phys. Chem. B* 113.18: 6378-396.

Porcal, P., Dillon P.J. and Molot L.A. (2013) Seasonal Changes in Photochemical Properties of Dissolved Organic Matter in Small Boreal Streams, *Biogeosciences* 10.8: 5533-543.

Kalinichev A.G., Iskrenova-Tchoukova E., Won-Young A., Clark M.M. and Kirkpatrick R.J. (2010) Effects of Ca2 on Supramolecular Aggregation of Natural Organic Matter in Aqueous Solutions: A Comparison of Molecular Modeling Approaches, *Geoderma* 169: 27-32.

Dash M.R. and Rajakumar B. (2012) Abstraction Kinetics of H-Atom by OH Radical from Pinonaldehyde (C 10 H 16 O 2): Ab Initio and Transition-State Theory Calculations, *A The Journal of Physical Chemistry A* 116.24: 5856-866.

Lundberg M., Kawatsu T., Vreven T., Frisch M.J. and Morokuma K. (2009) Transition States in a Protein Environment − ONIOM QM:MM Modeling of Isopenicillin N Synthesis, *Journal of Chemical Theory and Computation* 5.1: 222-34.

Andzelm J., Kölmel C. and Klamt A. (1995) Incorporation of Solvent Effects into Density Functional Calculations of Molecular Energies and Geometries, *The Journal of Chemical Physics* 103.21: 9312.

Jayathilaka P.B., Pathiraja G.C., Bandara A., Subasinghe N.D. and Nanayakkara N. (2014) Theoretical Study of Phenol and Hydroxyl Radical Reaction Mechanism in Aqueous Medium by the DFT/B3LYP/6-31 G(d,p)/CPCM Model, *Canadian Journal of Chemistry* 92.9: 809-13.

Torrent M., Vreven T., Musaev D.G, Morokuma K., Farkas Ö. and Schlegel H.B. (2002) Effects of the Protein Environment on the Structure and Energetics of Active Sites of Metalloenzymes. ONIOM Study of Methane Monooxygenase and Ribonucleotide Reductase, *Journal of the American Chemical Society* 124.2: 192-93.

Tanaka, N. and Itoh S. (2013) Density Functional Theory Studies on the Addition and Abstraction Reactions of OH Radical with Benzoate Anion, *Open Journal of Physical Chemistry* 03.01: 7-13.

Castaneda R., Cristina I., Alvarez-Idaboy J.R., Vivier-Bunge A. (2012) Rate Constants and Branching Ratios in the Oxidation of Aliphatic Aldehydes by OH Radicals under Atmospheric Conditions, *Journal of Mexican Chemical Society* 56(3),316-324.

Vreven T., Byun K.S., Komáromi I., Dapprich S., Montgomery J.A., Morokuma K. and Frisch M.J. (2003) Combining Quantum Mechanics Methods with Molecular Mechanics Methods in ONIOM, *Journal of Chemical Theory and Computation* 2.3: 815-26.

Kušić H., Rasulev B., Leszczynska D., Leszczynski J. and Koprivanac N. (2009) Prediction of Rate Constants for Radical Degradation of Aromatic Pollutants in Water Matrix: A QSAR Study. *Chemosphere* 75.8: 1128-134.

Borhani T.N.G., Saniedanesh M., Bagheri M. and Lim J.S. (2016) QSPR Prediction of the Hydroxyl Radical Rate Constant of Water Contaminants, *Water Research* 98: 344-53.

Jin X., Peldszus S. and Huck P.M. (2015) Predicting the Reaction Rate Constants of Micropollutants with Hydroxyl Radicals in Water Using QSPR Modeling. *Chemosphere* 138: 1-9.

Foresman J.B. and Frisch A.E. (1996) Exploring Chemistry with Electronic Structure Methods, Pittsburgh, PA: Gaussian.

Cramer C.J. (1961) Essentials of Computational Chemistry: Theories and Models. Chichester, West Sussex, England: Wiley & Sons.

Frisch M.J., Hratchian H.P. and Nielsen A.B. (2009) Gaussian 09 Programmer's Reference. Vol. 8. Wallingford, CT: Gaussian.

Wu P., Li J., Li S. and Tao F.M. (2011) Theoretical Study of Mechanism and Kinetics for the Addition of Hydroxyl Radical to Phenol, *Science China Chemistry* 55.2: 270-76.

Tanaka N. and Itoh S. (2013) Density Functional Theory Studies on the Addition and Abstraction Reactions of OH Radical with Benzoate Anion, *Open Journal of Physical Chemistry* 03.01: 7-13.

Bonin J., Janik I., Janik D. and Bartels D.M. (2007) Reaction of the Hydroxyl Radical with Phenol in Water Up to Supercritical Conditions, *The Journal of Physical Chemistry A* 111.10: 1869-1878.

Ramos B., Farah J.P.S. and Teixeira A.C.S.C. (2012) Estimating Reaction Constants by Ab Initio Molecular Modeling: A Study on the Oxidation of Phenol to Catechol and Hydroquinone in Advanced Oxidation Processes, *Brazilian Journal of Chemical Engineering* 29.1: 113-20.

Tomberg A., An introduction to Computational Chemistry and Avogadro Software, Gaussian 09W tutorial.

Weng Y. H., Wang Y.C., Tsai Y.T., Chuang C.J., Huang C.P. and Li K.C. (2012) Effect of Hydrophobicity of Humic Substances on Electro-ultrafiltration, *Desalination* 284: 128-34.

Snyder S.A., Westerhoff P., Yoon Y. and Sedlak D.L. (2003) Pharmaceuticals, Personal Care Products, and Endocrine Disruptors in Water: Implications for the Water Industry, *Environmental Engineering Science* 20.5: 449-69.

Amin M.T., Alazba A.A. and Manzoor U. (2014) A Review of Removal of Pollutants from Water/Wastewater Using Different Types of Nanomaterials, Advances in Materials Science and Engineering, 2014:24.

Gaussian 09, Revision E.01, Frisch M.J., Trucks G.W., Schlegel H.B., Scuseria, G.E., Robb, M.A., Cheeseman, J.R., Scalmani G., Baron V., Mennucci B., Petersson G.A., Nakatsuji H., Caricato M., Li X., Hratchian H.P., Izmaylov A.F., Bloino J., Zheng G., Sonnenberg J.L., Hada M., Ehara M., Toyota K., Fukuda R., Hasegawa J., Ishida M., Nakajima T., Honda Y., Kitao O., Nakai H., Vreven T., Montgomery J.A. Jr., Peralta J.E., Ogliaro F., Bearpark M., Heyd, J.J., Brothers E., Kudin K.N., Staroverov, V.N., Kobayashi R., Normand J., Raghavachari K., Rendell A., Burant J.C., Iyengar S.S., Tomasi J., Cossi M., Rega N., Millam J. M., Klene M., Knox J.E., Cross J.B., Bakken V., Adamo C., Jaramillo J., Gomperts R., Stratmann R.E., Yazyev O., Austin A.J., Cammi R., Pomelli C., Ochterski J.W., Martin R.L., Morokuma K., Zakrzewski V.G., Voth G.A., Salvador P., Dannenberg J.J., Dapprich S., Daniels A.D., Farkas Ö., Foresman, J.B., Ortiz J.V., Cioslowski J., Fox D.J., Gaussian, Inc., Wallingford CT, 2009.

Herrmann H., Hoffmann D., Schaefer T., Bräuer P. and Tilgner A. (2010) Tropospheric aqueous-phase free-radical chemistry: Radical sources, spectra, reaction kinetics and prediction tools, *Chem. Phys. Chem.*, 11, 3796–3822.

Hoffmann D., Weigert B., Barzaghi P. and Herrmann H. (2009) Reactivity of Poly-alcohols towards OH, NO3 and SO4− in Aqueous Solution, *Physical Chemistry Chemical Physics* 11.41: 9351.

Leenheer J.A. (1991) Organic substance structures that facilitate contaminant transport and transformations in aqueous sediments, In Baker R.A., ed., Organic Substances and Sediments in Water, Humics and Soils, Chelsea, MI, *Lewis Publishers*, 3-22.

Riley K. E., Op't Holt B.T. and Merz Jr. K. M. (2007) Critical Assessment of the Performance of Density Functional Methods for Several Atomic and Molecular Properties, *J Chem Theory Comput*. ; 3(2): 407–433. doi:10.1021/ct600185a.

Appendix A

A.1. Case Study: Calculation of the quenching ratios.

Given:

Concentration of atrazine(R) = 29.25ug/L

Molecular weight of atrazine= 215.68g/mol

C_R = 0.00002925 g/L or 1.35 x 10^{-7} mole/L

Reaction rate constant, k_R = 2.6 x 10^9 L / mol sec

Alkalinity = 288 mg/L

Hardness = 57 mg/L

$CaCO_3$ = 100.1 g/mol

$= \frac{Hardness}{1000 x CaCO3}$ = 0.000569431 mol/L

C_{HCO3-} = 0.000557926 mol/L

C_{H2CO3} = 6.28 x 10^{-6} mol/L

$C_{CO3(2-)}$ = 5.22 x 10^{-6} mol/L

$k_{CO3(2-)}$ = 3.90 x 10^8 L/mol s

k_{HCO3-} = 8.50 x 10^6 L/mol s

Total organic carbon (TOC) = 0.00257 mg/L

Molecular weight = 12g/mol

C_{TOC} = 0.0025 g/L (assumed)

C_{TOC} = 000208333mole/L

k_{NOM} = 3 x 10^8 L/mole s

$$Q_{NOM} = \frac{k_R C_R}{k_R C_R + k_{NOM} C_{NOM}} = 0.005610$$

$$Q_{Carbonate} = \frac{k_R C_R}{k_R C_R + k_{HCO3-} C_{HCO3-} + k_{CO3(2-)} C_{CO3(2-)}} = 0.05$$

Total Q = 0.005610+0.05 = 0.055056

$\%Q_{NOM} = \frac{0.005610}{0.055056}$ x 100 = 10.18%

$\%Q_{Carbonate} = \frac{0.05}{0.055056}$ x 100 = 89.81%

Reaction rate of each species:

$k_R C_R$ = 352.60 mol/Ls

$k_{NOM} C_{NOM}$ = 62500 mol/Ls

$k_{CO3(2-)}$ $C_{CO3(2-)}$ = 2036.17 mol/Ls

k_{HCO3-} C_{HCO3-} = 4742.37 mol/Ls

Appendix B

B.1. Bench Marking of Computational Method:

B.1.1. Introduction:

With the advancement in the computational theories and methods, it became necessary to access the performance and accuracy of the calculations for any molecular system. To overcome this issue, the benchmarking process was designed. In this process, a small model system was chosen that closely mimics the actual molecular system to be analyzed.

Test calculations were performed on this model system using different computational methods and computational demands and accuracy of different methods were studied.

For this study, phenol was chosen as the model system as it includes both an aromatic ring to practice HO• addition to the aromatic ring and alcohol to analyze the effect of functional group. Studies have been performed to analyze the reactivity of HO• with phenol using different computational methods.

B.1.2. Literature Review

A theoretical study was performed on the aqueous phase reactivity of HO• with phenol molecule by Jayathilaka et al., 2014. The reaction of phenol with HO• was a complex mechanism and the intermediates were found to be more harmful than their stable compounds. The stability of transition states and reaction products were calculated by relative molecular energies in the aqueous phase. For modeling the reaction between hydroxyl radical and phenol molecule, Gaussian03 software was used. Using the Density Functional Theory and CPCM with Becke-style 3 parameter Lee-Yang-Parr (B3LYP)

hybrid function and 6-31+G(d,p) basis set, four channels were studied namely HO• addition to ortho position, a meta position, para position and H-atom abstraction from the OH functional group. All the reactants, product radicals and transition states were optimized and harmonic frequencies were calculated on DFT/B3LYP/6-31+G(d,p) to check the position of optimized geometries on potential energy surface. Berny optimization method was used to optimize transition state. The CPCM solvation model was used to calculate the relative energy and rate constant calculations of the reaction at temperature 298.15K and water medium with dielectric constant ε= 878.39. One transition state was considered by having one imaginary frequency. The ortho addition product radical, para addition product radical, meta addition product radical and hydrogen abstraction product radical were four product radicals obtained from the reaction channel.

When hydroxyl radical attacked the ortho addition site of phenol, its C-C bond length increased for alternate carbon atoms in the ring. This happened because of the fact that electron density was transferred from the aromatic ring to the new C-O bond. It also shortened for the remaining carbon atoms of the ring. A similar pattern was observed for both meta -PR and para-PR product radicals.

The relative free energies were computed relative to the energy of the reactants. From the results, it was observed that the lowest relative energy was obtained from the ortho addition in transition state whereas H abstraction had the highest relative energy in the transition state. Since product radicals formed by addition reaction can form hydrogen bonds in the aqueous phase, they were stable than hydrogen abstraction reaction product

radical. In addition to that, the energy of the o-PR was less than that of m-PR and p-PR. So, o-PR was found to be most stable among all.

From the results, negative energies of ortho and para transition state implied that rate of the reactions was decreased. On comparing ortho and para reactions, the ortho reaction had a higher possibility of occurrence due to the higher negative activation energy.

The conclusions drawn from this study were as follows:

In this case, addition reaction was the most favorable reaction with the highest possibility of occurrence.

With the help of relative free energy data, it could be concluded that ortho position of the ring was the most active site for hydroxyl radicals.

PengZhen WU et al., 2011, theoretically analyzed the mechanism and kinetics for HO• addition to phenol. This reactivity was investigated under Gaussian 03 program. The density functional theory method with b3lyp/6-311++G(2dp,2df) basis set was used to obtain the transition states and products and complete basis set method using APNO basis set was used to study the addition reaction pathways. The reaction rate constants of the four reaction pathways were calculated using Transition State Theory within the temperature range of 210 to 360 K. Four reaction pathways included HO• addition to ortho carbon of the benzene ring, HO• addition to meta position, HO• addition to para position and HO• addition to ipso position. From the results, it was concluded that within the chosen temperature range, the addition of HO• to ortho position is dominant over all other reaction pathways.

Another study was performed by Nobuaki T. et al., 2013 on a compound nearly similar to phenol. This study focused on the kinetics and thermochemistry of the primary steps like OH radical addition to the benzoate anion and H-atom abstractions from the benzoate anion.

The geometries of the reactants, transition states, products, and complexes were optimized using the density functional theory (DFT) method. For the calculations, the basis set used was 6-311++G(2d,2p) and the hybrid GGA functionals like B3LYP and mPW1PW91, hybrid meta GGA functional like M06-2X and range-separated hybrid GGA functional CAM-B3LYP were used . Harmonic vibrational frequencies were calculated to verify the predicted structures as transition states .The obtained transition states were further investigated and confirmed under the subsequent calculation of intrinsic reaction coordinates. For the aqueous phase calculation, polarizable continuum method (IEF-PCM) was used. All these calculations were done under Gaussian 09.

The HO• could be added to five different sites of Benzoate anion namely carbonyl, ipso, ortho, meta and para carbons. The free energy of reaction, ΔrG value for the carbonyl addition obtained was positive while for other sites it was negative. The product obtained from carbonyl addition had its spin density located on the oxygen atoms of the OH added to COO group, whereas other products were delocalized to gain resonance stabilization energies. The ortho addition product was recognized as the most stable one thermodynamically, due to an intramolecular hydrogen bond between CO—HO with a bond length of 1.707(UmPW1PW91) to 1.816 (UM06-2X)A.

-

Distances elongated by 40% between C---OH in the transition states of ipso, ortho, meta and para addition reactions were found when compared with the products. This represented an early transition state achieved. However, in the carbonyl addition reaction, the difference between the equilibrium and the transition state C---OH distances was approximately 20% indicating late transition state achieved. The free energy of activation for the addition of OH to carbonyl carbon was found to be comparatively higher. The free energy of activation for the formation of $ortho_1$ and $para_1$ were the lowest. It was then concluded that ortho and para positions are the most favorable sites for the addition of HO radical. The total rate constants calculated for the OH addition into carbonyl, ipso. Ortho, meta and para were 5.2 x 10^{-12}, 1.1x10^{-12}, 7.3x10^{-13} and 3.2 x10^{-14} $cm^3mol^{-1}s^{-1}$ using UB3LYP, UmPW1PW91, UCAM-B3LYP and UM06-2X functionals respectively.

The H-atom abstraction at ortho and meta positions was carried out by optimizing the transition states using three different geometries where OH molecular axis was perpendicular to the molecular plane of benzoate anion or the OH molecular axis was in the plane of the benzoate anion with either O or H atom of the OH radical pointing towards carbonyl oxygen. The $TS_{ab\text{-}ortho1}$ was found to be planar with the OH---OC at a distance ranging from 1.650 A by mPW1PW91 to 1.704A by B3LYP. $TS_{ab\text{-}ortho2}$ was found to be nonplanar with OH pointing away from the carbonyl group. In the meta and para position H-atom abstraction in the TS structure, the OH molecular axis was found to be perpendicular to the plane of benzoate anion. The breaking bonds of C-H were found to be elongated by nearly 17, 14, 12, and 13% when compared with the equilibrium structures of benzoate anion. The forming O-H bonds were also elongated by 28, 35, 37 and 35% when compared with OH bond length of H_2O for $TS_{ab\text{-}ortho1}$, $TS_{ab\text{-}ortho2}$, $TS_{ab\text{-}meta}$ and $TS_{ab\text{-}}$

$_{para}$ respectively with UB3LYP. The free energy of activation for $TS_{ab\text{-}ortho1}$ obtained was smaller than TS_{ortho2}. The rate constants for H-atom abstractions via $TS_{ab\text{-}ortho1}$ was found to be larger than rate constants for other transition states. Total rate constants for abstraction reactions were $7x10^{-12}$, $4x10^{-12}$, $1.4x10^{-12}$ and $1.3x10^{-13}$ cm^3 $mol^{-1}s^{-1}$ using UB3LYP, UmPW1PW91, UCAM-B3LYP and UM06-2X respectively.

On comparing addition reaction with abstraction reaction, it was concluded that abstraction reaction was more favored reaction channel for HO and benzoate anion and hydrogen bonds in the transition states affects the reaction rates.

B.1.3. Methodology

The compound chosen for the benchmarking study was Phenol. This compound was chosen considering its small size, presence of an aromatic ring and alcohol as the functional group. The small size of phenol resulted in calculations to be less demanding in terms of computational costs and time. Aromatic ring and the functional group provided diversity for the evaluation. The theoretical investigation of reactivity of HO• with phenol was carried out using ab initio quantum mechanical calculations in both gas and an aqueous phase. These calculations were performed under Gaussian09 revision D.02 provided by Michigan Tech high-performance cluster "Superior" and also under the workstation established by Dr. Daisuke Minakata.

At first, the phenol molecule and HO• were drawn in the Gauss View 5.0.9 software and were optimized at the ground state for the gas phase. Using these optimized structures, transition state was drawn with a QST3 method for HO• attacking the ortho position of phenol. The reactants were placed at a distance of 1.6 A, the product formed

was HO• added to aromatic ring with a bond length of 1.45A and transition state at a distance of 1.49 A. The structure was optimized and frequency was calculated using different basis sets and functionals namely b3lyp/3-21+G*, b3lyp/6-31+G(d,p), b3lyp/6-311+G(3df,2p), b3pw91/6-31+G(d,p), MP2/6-31+G(d,p), MPWB1K/6-31+G(d,p), and M062X/6-31+G(d,p). Then, free energy of activation, $\Delta G^{act}_{gas,calc}$ was calculated using the following equation:

$$\Delta G^{act}_{gas,calc} = \text{Transition state } \Delta G_{gas,calc} - (\Delta G^{phenol}_{gas,calc} + \Delta G^{HO\bullet}_{gas,calc}) \quad (16)$$

Using the similar procedure, aqueous phase free energy of activation was also calculated with a minor difference of introduction of Universal Solvation Model-SMD.

B.1.4. Results and Discussions

Following the above methodology and calculations, results that have been obtained in both gas phase and the aqueous phase are tabulated in table 1. Also, it includes the free energy of activation values of phenol reaction with HO• reported in the literature.

Table 3: Calculated and reported free energy of activation for HO• addition to phenol at ortho position in gas and an aqueous phase.

Method	**ΔG activation (Gas phase) kcal/mol**	**ΔG activation (aqueous phase) kcal/mol**	**References**
b3lyp/3-21+G*	0.46	1.11	Calculated
b3lyp/6-31+G(d,p)	3.05	3.47	Calculated
b3lyp/6-311+G(3df,2p)	3.77	3.75	Calculated
b3pw91/6-31+G(d,p)	3.64	-5.88	Calculated
MP2/6-31+G(d,p)	13.51	14.39	Calculated
MPWB1K/6-31+G(d,p)	-8.54	-6.98	Calculated
M062X/6-31+G(d,p)	-8.14	-7.38	Calculated

G4(ortho position)		-4.42	(Minakata D. et al., 2011)
Experimental value using Eyring's equation		3.86	(Bonin et al., 2007)

From the table 3, it was observed that with the more computationally expensive method the free energy of activation in aqueous phase obtained was negative. However, as reported by Bonin et al., 2007 the experimental free energy of activation obtained was positive. This closely matched with our theoretically calculated free energy of activation obtained from DFT method using b3lyp/3-21+G*, b3lyp/6-31+G(d,p), and b3lyp/6-311+G(3df,2p) basis sets.

Our choice of the computational method and the basis set relied on the terms that it should be less demanding in terms of time and computational memory. This was due to the fact that the molecule to be used for the main study i.e; investigation of reactivity of HO• with different reactive sites of TNB model in aqueous was large with a total of 95 atoms. Performing theoretical calculations with computationally demanding method was not only highly time-consuming but it also required huge scratch space.

Hence, keeping in mind the accuracy requirement for the study, the time taken, the memory requirement and availability, we chose to proceed with the TD-DFT method utilizing b3lyp/3-21+G* basis set.

B.1.5. References

Javathilaka, Bhakthi.P, Pathiraja G.C., Bandara.A, Subhasinghe N.D, and Nanayakkara N. (2014) Theoretical Study of Phenol and Hydroxyl Radical Reaction Mechanism in Aqueous Medium by the DFT/B3LYP/6-31 G(d,p)/CPCM Model." *Canadian Journal of Chemistry Can. J. Chem.* 92.9 : 809-13.

Pengzhen W., Li.J, Li.S, and Tao F.M. (2011) Theoretical Study of Mechanism and Kinetics for the Addition of Hydroxyl Radical to Phenol *Science China Chemistry Sci. China Chem.* 55.2 : 270-76.

Tanaka, Nobuaki, and Shigeo Itoh. (2013) Density Functional Theory Studies on the Addition and Abstraction Reactions of OH Radical with Benzoate Anion. *Open Journal of Physical Chemistry OJPC* 03.01 : 7-13.

Bonin, Julien, Ireneusz J., Dorota J., and Bartels D.M. (2007). Reaction of the Hydroxyl Radical with Phenol in Water Up to Supercritical Conditions. *J. Phys. Chem. A The Journal of Physical Chemistry A* 111.10 : 1869-878.

Ramos, B., J. P. S. Farah, and A. C. S. C. Teixeira. (2012)Estimating Reaction Constants by Ab Initio Molecular Modeling: A Study on the Oxidation of Phenol to Catechol and Hydroquinone in Advanced Oxidation Processes. *Brazilian Journal of Chemical Engineering Braz. J. Chem. Eng.* 29.1 : 113-20.